Tumour immune rejection triggered by activation of α2-adrenergic receptors

Jingjing Zhu [1,2,3*], Stefan Naulaerts[1,2], Loubna Boudhan[1,2,3], Manon Martin[2,5], Laurent Gatto[2,5], and Benoit J. Van den Eynde[1,2,3,4]

[1] Ludwig Institute for Cancer Research, Brussels B-1200, Belgium.

[2] de Duve Institute, UCLouvain, Brussels B-1200, Belgium.

[3] Walloon Excellence in Life Sciences and Biotechnology, Brussels, Belgium.

[4] Ludwig Institute for Cancer Research, Nuffield Department of Clinical Medicine, University of Oxford, Oxford, United Kingdom.

[5]Computational Biology and Bioinformatics, Université catholique de Louvain, Brussels B-1200, Belgium.

* Correspondence and Lead Contact: Jingjing Zhu

Mailing address: Avenue Hippocrate, 75 B1.74.03 – B-1200 Brussels, BELGIUM

Phone number: 0032 2 764 75 80

Email address: jingjng.zhu@uclouvain.be

Immunotherapy based on immune checkpoint blocking (ICB) antibodies induces rejection of tumours and brings clinical benefit in patients with various cancer types[1]. However, tumours often resist immune rejection. Ongoing efforts trying to increase tumour response rates are based on combinations of ICB with compounds that aim to reduce immunosuppression in the tumour microenvironment (TME) but usually have little effect when used as monotherapies[2,3]. We show here that agonists of α2-adrenergic receptors (α2-AR) have surprisingly strong anti-tumour activity when used as monotherapies in multiple immunocompetent tumour models, including ICB-resistant models, but not in immunodeficient models. We also observed striking effects in human tumour xenografts implanted in mice reconstituted with human lymphocytes. The anti-tumour effects of α2-AR agonists were reverted by α2-AR antagonists, and were absent in α2a-AR knockout mice, demonstrating on-target action exerted on host cells, not tumour cells. Tumours from treated mice contained increased infiltrating T lymphocytes and reduced myeloid suppressor cells, which were more apoptotic. Single-cell RNA sequencing revealed upregulation of innate and adaptive immune response pathways in macrophages and T cells. To exert their anti-tumour effects, α2-AR agonists required $CD4^+$ T lymphocytes, $CD8^+$ T lymphocytes and macrophages. Reconstitution studies in α2a-AR knockout mice indicated that the agonists acted directly on macrophages, increasing their ability to stimulate T lymphocytes. Our results indicate that α2-AR agonists, some of which are available clinically, could significantly improve clinical efficacy of cancer immunotherapy.

Adrenergic receptors (ARs) are a class of G protein-coupled receptors. They are subdivided into two types (α and β) and several subtypes based on their structure, pharmacology, and signaling mechanisms[4]. β-adrenergic receptors (β-ARs) signal through Gs to increase adenylate

cyclase activity and cyclic AMP (cAMP) levels, resulting in activation of PKA and downstream transcription factors[5,6]. In contrast, α2-adrenergic receptors (α2-AR) signal through Gi to inhibit adenylate cyclase, reducing cAMP levels and PKA activity. Although adrenergic receptors have a well described role in the sympathetic nervous system, they are also expressed in other tissues and their function outside the nervous system is not well known, particularly for α2-AR. A number of immunosuppressive mechanisms acting in the TME to repress anti-tumour immune responses increase cAMP by activating adenylate cyclase. These include β-AR signaling but also adenosine receptor signaling, and prostaglandin signaling through EP2 and EP4 prostanoid receptors[7-9]. Relevant antagonists are being developed for cancer immunotherapy. We reasoned that α2-AR agonists, by inhibiting adenylate cyclase, might be more potent than such antagonists because they could simultaneously block multiple immunosuppressive pathways that increase cAMP.

Tumour growth inhibition by α2-AR agonists

To evaluate the role of α2-AR in cancer progression, we treated mice bearing MC38 colon tumours with different α2-AR agonists and antagonists. We initially tested guanabenz (GBZ) and observed a dramatic reduction of tumour growth and an increase of mice survival (Fig. 1a, Extended Data Fig. 1a). We then observed similar effects with two other a2-AR agonists, clonidine (CLD) and guanfacine (GFC) (Fig. 1a, Extended Data Fig. 1ab). In contrast, the α2-AR antagonists (yohimbine and phentolamine) did not affect tumour growth (Fig. 1a). We then tested 11 additional transplanted tumour models: melanomas B16F1 (Fig. 1b) and B16F10 (Extended Data Fig. 1ac), colorectal carcinomas MC38-OVA, lung carcinomas TC-1, hepatocellular carcinomas Hepa 1-6, T cell lymphomas E.G7-OVA, myelomas J558, mammary carcinomas

TS/A, renal carcinomas Renca, fibrosarcomas CMS5a, and mammary carcinomas 4T1 (Extended Data Fig. 1c). In all these models, we observed a similar inhibition of tumour growth upon treatment with α2-AR agonists.

Strikingly, several of the models that responded to α2-AR agonists are well known to be resistant to ICB, such as TC-1 (Extended Data Fig. 1c), B16F1 (Fig. 1b), B16F10 (Extended Data Fig. 1ac) and B16F10-OVA (Extended Data Fig. 1d). We further tested α2-AR agonists in the TiRP model of induced autochthonous melanoma, which was shown to resist all forms of immunotherapies[10,11]. Remarkably, all three α2-AR agonists showed anti-tumour effects in the TiRP model when used as monotherapies (Fig. 1c). Inhibition was even more significant when treatment started with smaller tumours (Extended Data Fig. 1e).

This effect appeared not to result from a direct action of α2-AR on tumour cells, as it was observed equally in tumour models that expressed very different levels of α2-AR (Extended Data Fig. 2a), and no direct growth inhibition was observed when tumour cells were treated with α2-AR agonists *in vitro* (Extended Data Fig. 2bc). Instead, tumour growth inhibition was immune-mediated, as it was not observed in immunodeficient NOD/Scid/Il-2rg$^{-/-}$ (NSG) mice (Fig. 1b). Accordingly, tumours from immunocompetent treated mice contained increased numbers of infiltrating CD8^{+} T lymphocytes (Fig. 1b, Extended Data Fig. 2d). Likewise, there was no effect of guanabenz when TiRP mice were in the immunodeficient background of *Rag1*-knockout mice, confirming a lymphocyte-mediated mechanism of action (Fig. 1c).

To explore the therapeutic effect of α2-AR agonists on human tumours, we tested them in immunodeficient NSG mice bearing human tumours and reconstituted with human allogeneic peripheral blood mononuclear cells (PBMCs). We injected NSG mice with cells from either human ovarian carcinomas SK-OV-3, human colorectal carcinomas LS411N, or human prostate carcinomas PC-3. Once tumour xenografts were established, we injected human PBMCs and

monitored tumour growth. In such models, tumour cells activate a response of human lymphocytes towards allogeneic antigens, which by nature are more immunogenic than tumour antigens. Despite this high immunogenicity, the allogeneic response failed to inhibit tumour growth, indicating the presence of immunosuppressive mechanisms in these tumours (Fig. 1d and Extended Data Fig. 3a). Thus, this model is convenient to evaluate therapeutic approaches aimed at modulating immunosuppression in the setting of human lymphocytes confronted to human tumours, without the hurdle of the poor immunogenicity of human tumours in the autologous setting[12]. We then repeated the experiment and started treating mice with guanabenz or clonidine at the time they received human PBMCs. We observed strong anti-tumour effects in all three models, indicating that α2-AR agonists can boost the rejection of human tumours by human lymphocytes (Fig. 1d and Extended Data Fig. 3ab). Importantly, despite expression of α2-AR by these tumours (Extended Data Fig. 3c), there was no effect in the absence of human PBMCs, confirming that the anti-tumour activity of α2-AR agonists was immune-mediated, and indicating that it was effective also on human lymphocytes. Indeed, xenografts from treated mice contained increased amounts of human tumour-infiltrating $CD8^+$ lymphocytes (Fig. 1d). Even though anti-tumour immune responses of cancer patients are weaker than the allogeneic responses tested here, these results suggest that the immune-mediated anti-tumour effects of α2-AR agonists could be translated to cancer patients.

Combination with checkpoint inhibitors

Mice treated with α2-AR agonists showed an increased expression of PD-1 in TILs and of PD-L1 on TME cells, in MC38-OVA, TC-1 and TiRP tumours (Fig. 1e). This prompted us to test combinations of α2-AR agonists with ICB. In the MC38-OVA model, which does respond to anti-PD-1, combination of anti-PD-1 with α2-AR agonists showed a strong synergistic anti-tumour effect, leading to complete tumour rejection in most mice (Fig. 1f, Extended Data Fig.

3d and 3e). In the TC-1 model, which does not respond to anti-PD-1 therapy, the addition of anti-PD-1 to α2-AR agonists slightly improved their anti-tumour effect (Fig. 1g and Extended Data Fig. 3f). Likewise, TiRP melanomas did not respond to combined ICB therapy (anti-CTLA4+anti-PD-1)[11], but the addition of combined ICB therapy improved the anti-tumour effect of guanabenz (Fig. 1h). Similar results were obtained in the CT26 and B16F1 models (Extended Data Fig. 3gh). Remarkably, in most ICB-resistant models tested, α2-AR agonists alone were already more efficient than ICB therapy.

Target validation of α2-AR

To confirm the on-target effect of α2-AR agonists, we first used α2-AR antagonist yohimbine, and found that coinjection of yohimbine with clonidine or guanabenz reverted almost completely the immune-mediated anti-tumour effect of these agonists on human tumour xenografts (Fig. 2a)[13]. Because α2a-AR was the most highly expressed α2-AR subtype in mouse tumours (Extended Data Fig. 3i), we then used *Adra2a*-KO mice[14], which are genetically deficient in α2a-AR (Extended Data Fig. 3j). The anti-tumour effect of clonidine and guanabenz on MC38 tumours was abolished in *Adra2a*-KO mice, and so was the increased infiltration of $CD8^+$ T cells (Fig. 2b). The anti-tumour effect of α2-AR agonists was also abolished in *Adra2a*-KO mice for three other models tested (MC38-OVA, TC-1 and B16F10-OVA) (Fig. 2c-e). Likewise, no synergistic effect was found for clonidine and guanabenz when combined with anti-PD-1 treatment in *Adra2a*-KO mice bearing MC38-OVA tumours (Fig. 2f). These results confirmed α2a-AR as the actual target of the agonists in mediating their anti-tumour effects. Of note, the tumours implanted in *Adra2a*-KO mice were wild-type for *Adra2a*. The fact that clonidine and guanabenz failed to inhibit tumour growth in *Adra2a*-KO mice therefore provided additional evidence that their anti-tumour effect was not linked to a direct action on tumour cells but relied on the host immune system. We further confirmed this notion by observing that the anti-tumour

145 effect of clonidine was fully maintained in wild-type mice bearing *Adra2a*-KO tumour cells
146 (Fig. 2g).
147 Alpha2-adrenergic receptors present in the brainstem exert negative feedback on preganglionic
148 neurons of sympathetic nerves, resulting in reduced release of noradrenaline by sympathetic
149 nerves and of adrenaline by adrenal glands[15,16]. This reduced sympathetic tone explains the
150 clinically effective antihypertensive effect of α2-AR agonists such as clonidine and guanabenz[17].
151 Several studies have described the immunosuppressive effect of signaling via the ß2-adrenergic
152 receptor (ß2-AR) acting on different cells of the TME[18-23]. It was therefore possible that the
153 immune potentiating effect of α2-AR agonists was indirect, through reduced ß2-AR signaling
154 resulting from the reduced sympathetic tone. However, this was excluded by the observation
155 that the anti-tumour effect of guanabenz was maintained in mice that were deficient for both
156 the ß1 and the ß2 adrenergic receptors (Fig. 2h)[24]. We concluded that α2-AR agonists do not
157 act via reduced ß2-AR signaling.

158 We then compared the anti-tumour efficacy of clonidine with that of propranolol, a ß2-AR an-
159 tagonist. We observed that clonidine was more potent than propranolol in the CT26 cancer
160 model (Fig. 2i). Propranolol was previously reported to increase the therapeutic efficacy of ICB
161 in the 4T1 and the B16F10 models, but showed little therapeutic anti-tumour activity as a mon-
162 otherapy[22,25]. This contrasts with the potent therapeutic effect of α2-AR agonists as a single
163 agent in multiple models, including 4T1 and B16F10 (Extended Data Fig. 1ac). Like adenosine
164 receptors and several prostaglandin receptors, ß2-AR associate with Gs and increase cAMP
165 production by adenylate cyclase. The increased anti-tumour potency of α2-AR agonists as com-
166 pared to propranolol is therefore in line with our hypothesis that α2-AR agonists, by inhibiting
167 cAMP production by adenylate cyclase, can block multiple pathways leading to cAMP-medi-
168 ated immunosuppression.

Role of CD4 and CD8 T cells

We further analyzed which immune cells drive the observed anti-tumour immune response, focusing on the MC38-OVA model, partially responsive to anti-PD-1 therapy, and the TC-1 model, an ICB-resistant model, both of which can grow in the C57/BL6J background of the *Adra2a*-KO mice. Given the increased $CD8^+$ TIL infiltration we observed in tumour models, we first asked whether the α2-AR agonists acted directly on $CD8^+$ T lymphocytes. Treating $CD8^+$ T cells *in vitro* with α2-AR agonists did not increase T cell proliferation or activation (Extended Data Fig. 4a). *In vivo*, the anti-tumour effect of clonidine required the presence of $CD8^+$ T cells, as it was partly reduced upon $CD8^+$ T-cell depletion in both models (Fig. 3a). However, $CD8^+$ T lymphocytes were not the primary targets of clonidine, because when we adoptively transferred wild-type OVA-specific OT-I $CD8^+$ T lymphocytes into *Adra2a*-KO mice bearing MC38-OVA we observed no increased tumour growth inhibition upon treatment with clonidine, despite the abundant presence of anti-tumour $CD8^+$ T cells expressing α2a-AR (Fig. 3b). As a control, clonidine increased MC38-OVA tumour growth inhibition in wild-type mice after adoptive transfer of OT-I $CD8^+$ T cells (Fig. 3c).

Besides an increased $CD8^+$ T-cell infiltration, we also observed an increased $CD8^+$ T-cell activity among TILs (Fig. 3d, Extended Data Fig. 2g). In addition, we also observed increased $CD4^+$ T-cell infiltration in the tumour, lymph nodes and spleen of clonidine-treated mice bearing TC-1 tumours (Fig. 3e). $CD4^+$ T cells were also increased in MC38-OVA tumours upon clonidine treatment (Extended Data Fig. 4b). Furthermore, blocking lymphocyte trafficking from secondary lymphoid organs to the tumour with FTY720 prevented the anti-tumour effect of clonidine (Fig. 3f), while the increased T-cell infiltration was reduced in the tumour and maintained in secondary lymphoid organs (Fig. 3e). Since $CD8^+$ T cells are required to mediate

192 the anti-tumour effect of α2-AR agonists, this result was not unexpected. However, the in-
193 creased T-cell infiltration induced by clonidine in secondary lymphoid organs of FTY720-
194 treated mice indicates that α2-AR agonists act not only in the tumour but also in the secondary
195 lymphoid organs. The relative role of each compartment remains to be determined.

196 **Role of MDSCs**

197 We previously observed in the TiRP melanoma model that $CD8^+$ TILs failed to survive in the
198 TME because of apoptosis triggered by Fas-ligand (FasL)-expressing polymorphonuclear my-
199 eloid-derived suppressor cells (PMN-MDSCs), now also termed pathologically activated neu-
200 trophils[26], which were enriched in these tumours[11]. We therefore asked whether α2-AR agonists
201 could prevent TILs apoptosis and favor TILs persistence in this model. We adoptively trans-
202 ferred TCRP1A $CD8^+$ T lymphocytes into TiRP mice bearing induced melanomas, which ex-
203 press the P1A tumour antigen. Agonists of α2-AR favoured the persistence of TCRP1A $CD8^+$
204 T lymphocytes in the tumours, reduced their apoptosis and increased their activity (Fig. 3g,
205 Extended Data Fig. 4c, Extended Data Fig. 2f). Furthermore, α2-AR agonists reduced the num-
206 ber of PMN-MDSC in the TME of TiRP tumours and increased their apoptosis (Fig. 3g, Ex-
207 tended Data Fig. 2d, Extended Data Fig. 4cde). This resulted in a synergistic therapeutic effect
208 of the combination of α2-AR agonists with adoptive transfer of anti-tumour $CD8^+$ T cells, which
209 was totally ineffective when administered alone in this model (Fig. 3h, Extended Data Fig. 4c).
210 We confirmed that α2-AR agonists also reduced TIL apoptosis and tended to reduce PMN-
211 MDSC numbers in the MC38 tumours, and observed that these effects were absent in *Adra2a*-
212 KO mice (Extended Data Fig. 4f).
213 To explore the mechanism of action of α2-AR agonists, we first performed a transcriptomic
214 analysis of bulk RNA from clonidine-treated and untreated MC38-OVA tumours from wild-
215 type and *Adra2a*-KO mice. Gene-set enrichment analysis (GSEA) identified an enrichment of

genes associated with the innate immune response, cell communication and cytokine response in treated tumours from wild-type mice (Fig. 3i). More specifically, treated tumours showed signs of immune stimulation, with a high expression of genes relevant for both the innate (such as genes encoding Tlr4[27], Tlr8, Tlr[28] or Cd36[29]) and adaptive immune response (Cd48[30], Itk[31], Ccl22[32], Nfatc1 or Nfatc2[33]) (Fig. 3j). These signs were absent in clonidine-treated tumours from *Adra2a*-KO mice (Fig. 3j). We confirmed by RT-qPCR the increased expression of *Tlr1, Tlr7, Tlr8*, *Ifnb1* and *Cxcl13* in tumours treated with clonidine and guanabenz in wild-type mice, but not in *Adra2a*-KO mice (Extended Data Fig. 4g).

Further UMAP analysis indicated transcriptomic changes in tumours from clonidine-treated mice that were similar to those of guanabenz-treated mice, and were absent in tumours from clonidine-treated *Adra2a*-KO mice (Extended Data Fig. 4h). Of note, tumours from guanabenz-treated *Adra2a*-KO mice showed a distinct transcriptomic profile, in line with the known effects of guanabenz on other pathways such as GADD34[34]. In contrast, the absence of transcriptomic changes induced by clonidine in *Adra2a*-KO mice indicated a higher specificity of clonidine for α2a-AR in this context. We therefore focused on clonidine for subsequent experiments.

Single-cell transcriptomic analysis

We then performed single-cell transcriptome analysis of the TME of MC38-OVA tumours (Extended Data Fig. 5a, Supplementary Table 1). We confirmed an increased infiltration of $CD8^+$ T lymphocytes upon clonidine treatment (Fig. 4ab). We also observed a decrease of the cell population expressing neutrophils markers, which might correspond to the PMN-MDSC we identified by flow cytometry. The most abundant population in the TME of these tumours were macrophages, which represented more than 87 % of $CD45^+$ cells (Fig. 4ab). These macrophages clustered into five different subsets (Fig. 4a, Extended Data Fig. 5bc). Upon clonidine

239 treatment, the dominant cluster Macrophages_3 was almost entirely replaced by cluster Mac-
240 rophages_1, while the other clusters were moderately altered (Fig. 4b). Clusters Macro-
241 phages_1 and _3 expressed a similar pattern of genes, but with differences in expression levels
242 (Extended Data Fig. 5c). Macrophages_1 showed an M1-macrophage like transcriptional pro-
243 file with high expression of MHC-class II related genes (*H2-eb1, H2-ab1)* and proinflammatory
244 genes (*Ccl2, Ccl3, Cxcl2, and Ccl4*), and was similar to the described *C1QC*$^{+}$ population of
245 tumour-associated macrophages, which were involved in phagocytosis and antigen presenta-
246 tion[35]. Macrophages_3 shows high expression of *Ccrl2* and *Cd83,* and expresses several proin-
247 flammatory genes (*Ccl2, Ccl3, Cxcl2, Ccl4*) similarly to Macrophages_1. However, as com-
248 pared to Macrophages_1, Macrophages_3 expresses lower levels of MHC-class II related genes
249 (*H2-eb1, H2-ab1*), as well as *Adgre1* (F4/80) and *Itgam* (CD11b). The major shift from Mac-
250 rophage_3 to Macrophage_1 that was induced by clonidine treatment might reflect an increased
251 proportion of activated macrophages able to phagocytose and present antigens. In line with this
252 hypothesis, a GSEA pathway analysis suggested that clonidine treatment increased overall mac-
253 rophage function, with enhanced antigen processing/cross-presentation and ER-phagosome
254 pathways, particularly in Macrophages_1 (Fig. 4c). RUNX family signaling was also increased
255 with clonidine, indicating a regulation of myeloid lineage differentiation[36]. Clonidine-induced
256 increased expression of several MHC-class II related genes, including *Cd74*, *H2-eb1* and *H2-*
257 *aa*, was confirmed, mostly in Macrophages_1 (Extended Data Fig. 5d). These results suggested
258 that clonidine not only increased the number of cells in Macrophages_1, but also improved their
259 ability to present antigens and interact with T cells. In line with this, using the CellPhoneDB
260 receptor ligand database, we observed a large increase in the number of significant interactions
261 between macrophages and CD8^{+} T cells upon clonidine treatment (Fig. 4d). This increase co-
262 incided with a significant enrichment in the expression of pathways linked to CD8^{+} T cell acti-

vation (Extended Data Fig. 5e). We found similar transcriptomic changes in macrophages infiltrating TC-1 lung tumours in mice treated with clonidine (Extended Data Fig. 5f). Altogether, these results suggested a key role of macrophages in mediating the effects of clonidine.

Involvement of macrophages

We then confirmed expression of α2a-AR by macrophages, MDSCs and $CD8^+$ T cells from the TME of MC38-OVA tumours (Extended Data Fig. 6a). Upon clonidine treatment, we observed by flow cytometry an increased macrophage infiltration with higher MHC II surface expression and increased phagocytic capacity in the TME of MC38-OVA tumours. These changes were not observed in tumours from *Adra2a*-KO mice (Fig. 4e, Extended Data Fig. 2d). Similar observations were made with guanabenz (Extended Data Fig. 6b), and also in the CT26 and TC-1 cancer models (Extended Data Fig. 6cd). This modulation of macrophages by α2-AR agonists suggested that macrophages could be the primary cell compartment acted upon by α2-AR agonists in mediating their anti-tumour effect.

To confirm their key role, we depleted macrophages in MC38-OVA tumour-bearing mice with clodronate liposomes, and we observed a reduced anti-tumour effect of clonidine along with a lack of TIL increase (Fig. 4f, Extended Data Fig. 6e). Of note, PMN-MDSCs were also reduced upon liposomal-clodronate treatment (Extended Data Fig. 6f). Furthermore, when we adoptively transferred wild-type macrophages into *Adra2a*-KO mice, we restored the anti-tumour effect of clonidine and the TIL increase (Fig. 4g). We validated that adoptively transferred macrophages do migrate into tumours and lymph nodes (Extended Data Fig. 6g, Extended Data Fig. 2e). These observations indicated the involvement of macrophages in the anti-tumour effect of α2-AR agonists.

In line with this, *in vitro* exposure of murine macrophages to α2-AR agonists enhanced their capacity to stimulate allogeneic $CD4^+$ and $CD8^+$ T cells (Extended Data Fig. 6h). Interestingly, while $CD4^+$ T cells were stimulated directly by clonidine-treated macrophages, the increased proliferation of $CD8^+$ T cells required the presence of $CD4^+$ T cells in the co-culture (Extended Data Fig. 6h). Likewise, when we co-cultured ovalbumin-pulsed syngeneic macrophages with OVA-specific $CD4^+$ (OT-II) and $CD8^+$ (OT-I) T cells, we observed increased proliferation of both upon clonidine treatment (Extended Data Fig. 6i, Extended Data Fig. 2h), and increased interferon-gamma (Ifn-γ) production by OT-I $CD8^+$ T cells (Extended Data Fig. 6j, Extended Data Fig. 2g). These effects were blocked by anti-MHC II antibodies and were absent in co-cultures with *Adra2a-KO* macrophages. *In vivo*, depletion of $CD4^+$ T cells in the TC-1 model abolished the anti-tumour effect of clonidine (Extended Data Fig. 7ab) and the increased $CD8^+$ T-cell infiltration in the tumour and in secondary lymphoid organs (Extended Data Fig. 7c), further supporting the critical role of $CD4^+$ T cells in mediating the effects of α2-AR agonists. Similarly, the anti-tumour effect of clonidine in both the TC-1 and the MC38-OVA models was attenuated in mice treated with MHC-class II blocking antibody (Extended Data Fig. 7de). These results are in line with a model in which α2-AR agonists activate macrophages to stimulate $CD4^+$ T lymphocytes, which then further activate $CD8^+$ T lymphocytes. In line with this, single-cell analysis of TC-1 tumours from mice treated with clonidine revealed a strong increase of $CD4^+$ T cells (Extended Data Fig. 5f).

Alpha2-AR activation inhibits adenylate cyclase, resulting in decreased production of cAMP and reduced PKA activity. We confirmed reduced PKA activity in myeloid cells isolated from tumours and lymph nodes from mice treated with clonidine (Extended Data Fig. 8a, left panels). These cells also showed increased MHC II expression (Extended Data Fig. 8a, right panels). Likewise, *in vitro* differentiated M1 macrophages exposed to clonidine showed reduced cAMP levels (Extended Data Fig. 8b). They also showed reduced PKA activity and increased MHC II

expression, both of which were not observed in *Adra2a*-KO macrophages (Extended Data Fig. 8c). However, it remains to be determined whether the anti-tumour effects of α2-AR agonists are mediated by the cAMP-PKA pathway, either entirely or partially, and which downstream pathways are involved.

Translational relevance

We further evaluated the translational relevance of our findings. Based on the clinical data from TCGA, a Kaplan–Meier survival analysis showed a significant association between a high expression of α2-AR and a better overall survival and progression-free survival in lung adenocarcinoma patients (Extended Data Fig. 9a). However, there were only modest positive correlations between α2-AR expression and multiple immunomodulatory molecules (Extended Data Fig. 9b). It is important to note that α2-AR expression per se may not suffice to trigger signaling if there is no ligand. We therefore evaluated whether there was a link between α2-AR signaling in human tumours and response to immunotherapy. To do so, we established an α2-AR activation signature based on our bulk mouse transcriptomics data. This signature consists of two components that are either upregulated (Post_Up) or downregulated (Post_Down) upon α2-AR treatment (Extended Data Fig. 9c, Supplementary Table 2). We then queried the impact of these two signature sets (human ortholog genes) on clinical response to anti-PD-1 and anti-PD-L1 immunotherapy using TIDE (Extended Data Fig. 9d). Interestingly, for anti-PD-L1 treatment in metastatic urothelial carcinoma[37], we observed a worse survival associated with a high expression of the downregulated set ($p=2.67x10^{-2}$) (Extended Data Fig. 9d left panel). High expression of the upregulated set was associated with better outcomes of anti-PD-1 therapy in a melanoma trial[38] ($p=1.03x10^{-2}$) (Extended Data Fig. 9d right panel). The α2-AR activation signature also correlated with macrophage infiltration, T-cell infiltration, TCR richness, and IFN-

γ response in all human tumours from the TCGA data set (Extended Data Fig. 9e). These observations suggest that α2-AR signaling induces transcriptomic changes that correlate with a better response to immunotherapy. This further supports the translational potential of our findings.

Altogether, our results provide evidence that agonists of the α2-AR increase anti-tumour immune responses by modulating myeloid cells in the TME, and could be exploited for cancer immunotherapy. Of note, previous reports described increased proliferation of some tumour cell lines exposed to α2-AR agonists[39,40], while other reports found opposite effects[41,42]. In some *in vivo* experiments also, treatment with α2-AR agonists favored metastasis development[43,44]. The results we report here in multiple tumour models, both *in vitro* and *in vivo*, do not confirm these early observations. One potential explanation for these divergent results is the dose: we used a dose of 5 mg/kg for the *in vivo* experiments, which is higher than the dose used in the previous studies (3-100 µg/kg). It is possible that the immune-mediated anti-tumour effects we report here require such high doses, and therefore were not captured in previous experiments. Indeed, the anti-tumour effect was not maintained when a tenfold reduced dose was used in daily i.p. injections (Extended Data Fig. 1b). Of note, we observed a similar anti-tumour effect upon delivery of clonidine by the oral route in the drinking water as compared to daily *i.p.* injections (Extended Data Fig. 10ab).

Discussion

The functional interplay between the autonomous nervous system and the immune system has been highlighted recently, particularly in the context of cancer[15,18,45-47]. In particular, modulation of anti-tumour immunity by the adrenergic system was reported for ß2-adrenergic signaling, which acts on several TME cell types to suppress immune responses[20,22,48]. Accordingly, ß2-AR antagonists were found to potentiate ICB therapy, and are currently tested in clinical

trials[23]. We show here that the signal induced by α2-ARs is opposite, since their activation stimulates anti-tumour immunity. This is likely related to the opposite action of ß2-ARs and α2-ARrs on secondary signals. While ß2-ARs increase cAMP by activating adenylate cyclase through protein Gs, α2-ARs signal through inhibitory protein Gi to inhibit adenylate cyclase and reduce cAMP levels. Previous work indicated that alpha-adrenergic signaling limited the development of MDSC: chemical disruption of sympathetic signaling with a neurotoxin favored MDSC development and suppressed anti-tumour immunity[47]. Our results are in line with these observations, as we see a reduction of MDSC in the TME upon treatment with α2-AR agonists. We further highlight a direct effect of α2-AR agonists on macrophages, which appear to be their main cellular targets in the TME. Because $CD4^+$ and $CD8^+$ T lymphocytes are required for the anti-tumour effect and are enriched in the TME upon treatment, it appears that the α2-AR agonists activate macrophages to better recruit and activate $CD4^+$ and $CD8^+$ T lymphocytes in the TME. See Extended Data Fig. 10c for a schematic model of the anti-tumour effect of α2-AR agonists.

The relative role of macrophages and PMN-MDSC in the anti-tumour effects of α2-AR agonists may vary according to the tumour model. In the TiRP model, we know from previous work that PMN-MDSC are highly enriched and play a dominant suppressive role, by inducing TIL apoptosis via FasL[11]. Therefore, the reduction of PMN-MDSC numbers likely plays an important role to mediate the effects of α2-AR agonists in this model. But macrophages may also contribute. In the MC38-OVA model, tumour-associated macrophages are highly abundant, and we observed striking phenotypic and transcriptomic changes in macrophages from treated MC38-OVA tumours, suggesting a prominent role of macrophages in this model. But PMN-MDSC were also reduced in numbers by clonidine in MC38-OVA and MC38 tumours, and this likely also contributed to promoting tumour rejection by $CD8^+$ T lymphocytes. Besides MDSC and

macrophages, it is not impossible that α2-AR agonists also act on other cell types that contribute to their anti-tumour effects. Further work will be required to address this.

Importantly, we observed potent therapeutic efficacy of α2-AR agonists used as monotherapy in multiple tumour models, including humanized models and models that are totally resistant to current approaches of cancer immunotherapy. Such agonists have been used for decades in humans to treat high blood pressure. Their pharmacology and safety profile are well known. Despite the likely need to use higher doses than previously and to mitigate sedative effects, our findings warrant the clinical testing of α2-AR agonists in cancer patients.

References:

1 Ribas, A. & Wolchok, J. D. Cancer immunotherapy using checkpoint blockade. *Science* **359**, 1350-1355, doi:10.1126/science.aar4060 (2018).

2 Marin-Acevedo, J. A., Kimbrough, E. O. & Lou, Y. Next generation of immune checkpoint inhibitors and beyond. *J. Hematol. Oncol.* **14**, 45, doi:10.1186/s13045-021-01056-8 (2021).

3 Rotte, A., Jin, J. Y. & Lemaire, V. Mechanistic overview of immune checkpoints to support the rational design of their combinations in cancer immunotherapy. *Ann. Oncol.* **29**, 71-83, doi:10.1093/annonc/mdx686 (2018).

4 Giovannitti, J. A., Jr., Thoms, S. M. & Crawford, J. J. Alpha-2 adrenergic receptor agonists: a review of current clinical applications. *Anesth Prog* **62**, 31-39, doi:10.2344/0003-3006-62.1.31 (2015).

5 Kim, T. J., Sun, J., Lu, S., Zhang, J. & Wang, Y. The regulation of beta-adrenergic receptor-mediated PKA activation by substrate stiffness via microtubule dynamics in human MSCs. *Biomaterials* **35**, 8348-8356, doi:10.1016/j.biomaterials.2014.06.018 (2014).

6 Sucharov, C. C., Dockstader, K., Nunley, K., McKinsey, T. A. & Bristow, M. beta-Adrenergic receptor stimulation and activation of protein kinase A protect against alpha1-adrenergic-mediated phosphorylation of protein kinase D and histone deacetylase 5. *J Card Fail* **17**, 592-600, doi:10.1016/j.cardfail.2011.03.006 (2011).

7 Wang, W. & Cao, X. Beta-Adrenergic Signaling in Tumor Immunology and Immunotherapy. *Crit. Rev. Immunol.* **39**, 93-103, doi:10.1615/CritRevImmunol.2019031188 (2019).

8 Allard, B., Allard, D., Buisseret, L. & Stagg, J. The adenosine pathway in immuno-oncology. *Nat Rev Clin Oncol* **17**, 611-629, doi:10.1038/s41571-020-0382-2 (2020).

9 Ching, M. M., Reader, J. & Fulton, A. M. Eicosanoids in Cancer: Prostaglandin E2 Receptor 4 in Cancer Therapeutics and Immunotherapy. *Frontiers in pharmacology* **11**, 819, doi:10.3389/fphar.2020.00819 (2020).

10 Huijbers, I. J. *et al.* An inducible mouse model of melanoma expressing a defined tumor antigen. *Cancer Res.* **66**, 3278-3286 (2006).

11 Zhu, J. *et al.* Resistance to cancer immunotherapy mediated by apoptosis of tumor-infiltrating lymphocytes. *Nat. Commun.* **8**, 1404 (2017).

12 Hennequart, M. *et al.* Constitutive IDO1 Expression in Human Tumors Is Driven by Cyclooxygenase-2 and Mediates Intrinsic Immune Resistance. *Cancer Immunol. Res.* **5**, 695-709, doi:10.1158/2326-6066.CIR-16-0400 (2017).

13 Hedner, T. *et al.* Yohimbine pharmacokinetics and interaction with the sympathetic nervous system in normal volunteers. *Eur. J. Clin. Pharmacol.* **43**, 651-656, doi:10.1007/BF02284967 (1992).

14 Altman, J. D. *et al.* Abnormal regulation of the sympathetic nervous system in alpha2A-adrenergic receptor knockout mice. *Molecular pharmacology* **56**, 154-161, doi:10.1124/mol.56.1.154 (1999).

15 Godinho-Silva, C., Cardoso, F. & Veiga-Fernandes, H. Neuro-Immune Cell Units: A New Paradigm in Physiology. *Annual review of immunology* **37**, 19-46, doi:10.1146/annurev-immunol-042718-041812 (2019).

16 Starke, K., Endo, T. & Taube, H. D. Relative pre- and postsynaptic potencies of alpha-adrenoceptor agonists in the rabbit pulmonary artery. *Naunyn Schmiedebergs Arch Pharmacol* **291**, 55-78, doi:10.1007/BF00510821 (1975).

17 MacMillan, L. B., Hein, L., Smith, M. S., Piascik, M. T. & Limbird, L. E. Central hypotensive effects of the alpha2a-adrenergic receptor subtype. *Science* **273**, 801-803, doi:10.1126/science.273.5276.801 (1996).
18 Zahalka, A. H. & Frenette, P. S. Nerves in cancer. *Nat Rev Cancer* **20**, 143-157, doi:10.1038/s41568-019-0237-2 (2020).
19 Yang, J. H., Lee, E. O., Kim, S. E., Suh, Y. H. & Chong, Y. H. Norepinephrine differentially modulates the innate inflammatory response provoked by amyloid-beta peptide via action at beta-adrenoceptors and activation of cAMP/PKA pathway in human THP-1 macrophages. *Exp Neurol* **236**, 199-206, doi:10.1016/j.expneurol.2012.05.008 (2012).
20 Wu, J. J. *et al.* G protein-coupled receptor kinase 2 regulating beta2-adrenergic receptor signaling in M2-polarized macrophages contributes to hepatocellular carcinoma progression. *Onco Targets Ther* **12**, 5499-5513, doi:10.2147/OTT.S209291 (2019).
21 Qiao, G. *et al.* beta-Adrenergic signaling blocks murine CD8(+) T-cell metabolic reprogramming during activation: a mechanism for immunosuppression by adrenergic stress. *Cancer Immunol Immunother* **68**, 11-22, doi:10.1007/s00262-018-2243-8 (2019).
22 Mohammadpour, H. *et al.* beta2 adrenergic receptor-mediated signaling regulates the immunosuppressive potential of myeloid-derived suppressor cells. *J Clin Invest* **129**, 5537-5552, doi:10.1172/JCI129502 (2019).
23 Gandhi, S. *et al.* Phase I Clinical Trial of Combination Propranolol and Pembrolizumab in Locally Advanced and Metastatic Melanoma: Safety, Tolerability, and Preliminary Evidence of Antitumor Activity. *Clin Cancer Res* **27**, 87-95, doi:10.1158/1078-0432.CCR-20-2381 (2021).
24 Rohrer, D. K., Chruscinski, A., Schauble, E. H., Bernstein, D. & Kobilka, B. K. Cardiovascular and metabolic alterations in mice lacking both beta1- and beta2-adrenergic receptors. *J Biol Chem* **274**, 16701-16708, doi:10.1074/jbc.274.24.16701 (1999).
25 Kokolus, K. M. *et al.* Beta blocker use correlates with better overall survival in metastatic melanoma patients and improves the efficacy of immunotherapies in mice. *Oncoimmunology* **7**, e1405205, doi:10.1080/2162402X.2017.1405205 (2018).
26 Kim, R. *et al.* Ferroptosis of tumour neutrophils causes immune suppression in cancer. *Nature* **612**, 338-346, doi:10.1038/s41586-022-05443-0 (2022).
27 Fukata, M. *et al.* Innate immune signaling by Toll-like receptor-4 (TLR4) shapes the inflammatory microenvironment in colitis-associated tumors. *Inflamm Bowel Dis* **15**, 997-1006, doi:10.1002/ibd.20880 (2009).
28 Medzhitov, R. Toll-like receptors and innate immunity. *Nat Rev Immunol* **1**, 135-145, doi:10.1038/35100529 (2001).
29 Park, L. *et al.* Innate immunity receptor CD36 promotes cerebral amyloid angiopathy. *Proc Natl Acad Sci U S A* **110**, 3089-3094, doi:10.1073/pnas.1300021110 (2013).
30 McArdel, S. L., Terhorst, C. & Sharpe, A. H. Roles of CD48 in regulating immunity and tolerance. *Clin Immunol* **164**, 10-20, doi:10.1016/j.clim.2016.01.008 (2016).
31 Readinger, J. A., Mueller, K. L., Venegas, A. M., Horai, R. & Schwartzberg, P. L. Tec kinases regulate T-lymphocyte development and function: new insights into the roles of Itk and Rlk/Txk. *Immunol Rev* **228**, 93-114, doi:10.1111/j.1600-065X.2008.00757.x (2009).
32 Ushio, A. *et al.* CCL22-Producing Resident Macrophages Enhance T Cell Response in Sjogren's Syndrome. *Frontiers in immunology* **9**, 2594, doi:10.3389/fimmu.2018.02594 (2018).

33 Peng, S. L., Gerth, A. J., Ranger, A. M. & Glimcher, L. H. NFATc1 and NFATc2 together control both T and B cell activation and differentiation. *Immunity* **14**, 13-20, doi:10.1016/s1074-7613(01)00085-1 (2001).
34 Tsaytler, P., Harding, H. P., Ron, D. & Bertolotti, A. Selective inhibition of a regulatory subunit of protein phosphatase 1 restores proteostasis. *Science* **332**, 91-94, doi:10.1126/science.1201396 (2011).
35 Zhang, L. *et al.* Single-Cell Analyses Inform Mechanisms of Myeloid-Targeted Therapies in Colon Cancer. *Cell* **181**, 442-459 e429, doi:10.1016/j.cell.2020.03.048 (2020).
36 Voon, D. C., Hor, Y. T. & Ito, Y. The RUNX complex: reaching beyond haematopoiesis into immunity. *Immunology* **146**, 523-536, doi:10.1111/imm.12535 (2015).
37 Mariathasan, S. *et al.* TGFbeta attenuates tumour response to PD-L1 blockade by contributing to exclusion of T cells. *Nature* **554**, 544-548, doi:10.1038/nature25501 (2018).
38 Gide, T. N. *et al.* Distinct Immune Cell Populations Define Response to Anti-PD-1 Monotherapy and Anti-PD-1/Anti-CTLA-4 Combined Therapy. *Cancer Cell* **35**, 238-255 e236, doi:10.1016/j.ccell.2019.01.003 (2019).
39 Castillo, L. F., Rivero, E. M., Goffin, V. & Luthy, I. A. Alpha2-adrenoceptor agonists trigger prolactin signaling in breast cancer cells. *Cellular signalling* **34**, 76-85, doi:10.1016/j.cellsig.2017.03.003 (2017).
40 Christensen, L. A., Finch, R. A., Booker, A. J. & Vasquez, K. M. Targeting oncogenes to improve breast cancer chemotherapy. *Cancer Res* **66**, 4089-4094, doi:10.1158/0008-5472.CAN-05-4288 (2006).
41 Kanno, N. *et al.* Stimulation of alpha2-adrenergic receptor inhibits cholangiocarcinoma growth through modulation of Raf-1 and B-Raf activities. *Hepatology* **35**, 1329-1340, doi:10.1053/jhep.2002.33330 (2002).
42 Maccari, S. *et al.* alpha-Adrenoceptor stimulation attenuates melanoma growth in mice. *Br J Pharmacol* **179**, 1371-1383, doi:10.1111/bph.15731 (2022).
43 Szpunar, M. J., Burke, K. A., Dawes, R. P., Brown, E. B. & Madden, K. S. The antidepressant desipramine and alpha2-adrenergic receptor activation promote breast tumor progression in association with altered collagen structure. *Cancer Prev Res (Phila)* **6**, 1262-1272, doi:10.1158/1940-6207.CAPR-13-0079 (2013).
44 Lavon, H. *et al.* Dexmedetomidine promotes metastasis in rodent models of breast, lung, and colon cancers. *Br J Anaesth* **120**, 188-196, doi:10.1016/j.bja.2017.11.004 (2018).
45 Grebe, K. M. *et al.* Sympathetic nervous system control of anti-influenza CD8+ T cell responses. *Proc. Natl. Acad. Sci. USA* **106**, 5300-5305, doi:0808851106 [pii] 10.1073/pnas.0808851106 (2009).
46 Eng, J. W. *et al.* A nervous tumor microenvironment: the impact of adrenergic stress on cancer cells, immunosuppression, and immunotherapeutic response. *Cancer Immunol Immunother* **63**, 1115-1128, doi:10.1007/s00262-014-1617-9 (2014).
47 Nevin, J. T., Moussa, M., Corwin, W. L., Mandoiu, II & Srivastava, P. K. Sympathetic nervous tone limits the development of myeloid-derived suppressor cells. *Sci Immunol* **5**, doi:10.1126/sciimmunol.aay9368 (2020).
48 Qiao, G. *et al.* Chronic Adrenergic Stress Contributes to Metabolic Dysfunction and an Exhausted Phenotype in T Cells in the Tumor Microenvironment. *Cancer immunology research* **9**, 651-664, doi:10.1158/2326-6066.CIR-20-0445 (2021).

Figure legends

Fig. 1: Alpha2-AR agonists induce immune-mediated tumour regression in multiple models. **a**, Progression of colon carcinomas MC38 in mice treated with vehicle (Con), α2-AR agonists guanabenz (GBZ), clonidine (CLD) or guanfacine (GFC), or with α2-AR antagonists yohimbine (YHB) or phentolamine (PHE). **b**, Progression of B16F1 melanomas in immunocompetent (left panels) or immunodeficient (NSG, right panels) mice treated with vehicle, GBZ, CLD or GFC. $CD8^+$ T-cell infiltration was analysed by flow cytometry on tumours at the time of sacrifice (middle panel). **c**, Progression of induced melanomas in wild-type or immunodeficient TiRP mice treated with vehicle, GBZ, CLD or GFC. **d**, Progression and $CD8^+$ T-cell infiltration of human ovarian cancers SK-OV-3 in NSG mice treated with vehicle, GBZ or CLD after adoptive transfer of allogeneic human PBMC. **e**, Expression of PD-1 on tumour-infiltrating $CD8^+$ T cells (top) and of PD-L1 on total living cells (bottom) from MC38-OVA , TC-1 and TiRP tumours in mice treated with CLD or GBZ. **f-h**, Progression of MC38-OVA (f), TC-1 (g) and induced TiRP tumours (h) in mice treated with GBZ, CLD, ICB (anti-PD-1 or anti-PD-1+anti-CTLA4), or combinations. Treatments started on day 0 (7 days after tumour implantation) (a, b, f and g), or when tumours were established as indicated (c, d, h). Drugs were administered daily by i.p. injections: GBZ, CLD, YHB, PHE, 5 mg/kg, GFC, 2 mg/kg. Anti-CTLA4 (40 µg) and/or anti-PD-1 (200 µg) antibodies (i.p.) were given 1 day before the first injection of α2-AR agonists, then twice a week. Number of mice indicated in brackets. Data (mean ± s.e.m) from one representative experiment out of at least two (except for (c, f and g): all mice shown, for h: data pooled from two independent experiments). P values determined by: ordinary two-way ANOVA (a-d, f-h), Unpaired *t*-test, two-tailed (columns, b,d,e); **** $p<0.0001$.

Fig. 2: Validation of α2-AR as the target mediating the anti-tumour effects of agonists. a, Human colorectal cancer xenografts LS411N in NSG mice reconstituted with human PBMC and treated with clonidine (CLD) or guanabenz (GBZ), and/or yohimbine (YHB). **b**, Colon carcinomas MC38 in wild-type or *Adra2a*-KO mice treated with vehicle, CLD or GBZ. $CD8^+$ T-cell infiltration was analysed as above. **c-e**, MC38-OVA colon carcinomas (c), TC-1 lung carcinomas (d) and B16F10-OVA melanomas (e) in wild-type or *Adra2a*-KO mice treated with vehicle, GBZ or CLD. **f**, Tumour growth (left) and mouse survival (right) of colon carcinomas MC38-OVA in *Adra2a*-KO mice treated with CLD, GBZ and/or anti-PD-1, as indicated. **g,** Control or *Adra2a*-KO TC-1 lung carcinomas progression in wild-type mice treated with vehicle or CLD. **h**, Colon carcinomas MC38 in wild-type or *Adrb1/Adrb2*-KO mice treated with vehicle or GBZ. **i**, Colon carcinomas CT26 in mice treated with vehicle, propranolol (PRP), CLD or both. Drugs were administered daily by i.p. injection: GBZ, CLD, PRP: 5 mg/kg; YHB 10 mg/kg. Treatments started on day 0, when tumours were well established as indicated on the graphs (a,c-h), or 7 days after tumour implantation (b and i). Anti-PD-1 (200 µg) antibodies (i.p.) were given 1 day before the first injection of α2-AR agonists, and then twice a week. Data (mean ± s.e.m) from one representative experiment out of at least two performed (except for (e, f and g): all mice shown). Number of mice per group indicated in brackets. P values determined by ordinary two-way ANOVA (a-i), *t*-test (Unpaired, two-tailed) (column, b). Log-rank (Mantel-Cox) test was used for the statistical evaluation of mouse survival (f, right panel). **** $p<0.0001$.

Fig. 3: Modulation of $CD8^+$ T cells and MDSCs by α2-AR agonists. a, Tumour progression in mice depleted of $CD8^+$ T cells and treated with CLD. **b**, MC38-OVA tumours in *Adra2a*-KO mice receiving adoptive cell therapy (ACT) of 10^7 *in vitro* activated OVA-specific TCR-

OT1 $CD8^+$ T cells, and treated with CLD. **c**, Same as (b) but in wild-type mice. **d,** Intracellular Tnf-α (top) and Ifn-γ (bottom) in $CD8^+$ T cells infiltrating TC-1 tumours. **e,** $CD4^+$ and $CD8^+$ T-cell infiltration in TC-1 tumours, lymph nodes and spleens analyzed by flow cytometry after 7 days of CLD and/or FTY720. **f,** Progression of TC-1 tumours in mice treated with CLD, FTY720 or both. **g**, Infiltration, activation, and apoptosis of P1A-specific $CD8^+$ T cells and PMN-MDSCs in P1A-expressing TiRP melanomas in mice treated with GBZ for 7 days after ACT of 10^7 activated TCRP1A $CD8^+$ T cells. **h**, Progression of induced TiRP melanomas upon GBZ treatment after ACT as in (g). **i**, Bulk RNAseq GSEA plot for CLD-treated vs untreated MC38-OVA tumours from wild-type or *Adra2a*-KO mice (4 groups, n=3 per group). Higher normalized enriched scores (NES) indicate upregulation in treated mice. P-values and FDR calculated using standard GSEA permutation-based approach, with 1000 iterations. Significant enrichments circled in bold (FDR<0.05). **j**, Bulk RNAseq: Heatmap of gene expression in treated tumours vs control post DESeq2 analysis. A zoomed-in color scale is shown for the KO group. GBZ, CLD: 5 mg/kg i.p. daily. FTY720: 10 μg per mouse, i.p. daily, starting one day before agonist treatment. CD8-depletion antibody: 500 μg day -1, then 150 μg weekly. Treatments started on day 0, when tumours were established as indicated. Data (mean ± s.e.m) from one representative experiment out of at least two (a-right,b,c,f,h), except for (a-left,d,e,g): all mice shown. P values determined by ordinary two-way ANOVA (a,b,c,f,h), *t*-test (Unpaired, two-tailed) (d,e,g). **** $p<0.0001$.

Fig 4: Role of macrophages in the anti-tumour effect of α2-AR agonists. a, UMAP representation of scRNAseq of untreated (left) and CLD-treated MC38-OVA tumours (right); pools of 10 mice per group. Leiden clusters were identified with PhenoGraph, (n_neighbours=25,

612 n_principal_components=26). **b**, Relative abundances of immune cells per cluster. Cell identi-
613 ties were assigned based on published lists of markers (Supplementary Table 1). **c**, Set enrich-
614 ment per population for relevant pathways. Significant terms marked with black circle. Marker
615 size represents p-value, color intensity indicates normalized enrichment score (NES). P-values
616 and FDR obtained by randomly permutating gene ranks 1000 times and testing with GSEA
617 approach. **d**, Receptor-ligand interactions between macrophages (donor) and $CD8^+$ T cells (re-
618 ceptor) identified by CellPhoneDB. **e**, Infiltration (n=10), surface MHC II expression (n=10)
619 and phagocytic activity (n=8) of TME macrophages from wild-type or *Adra2a*-KO mice treated
620 with CLD. **f,** Left: Progression of MC38-OVA tumours in macrophage-depleted mice treated
621 with CLD. Middle: Relative size of CLD-treated tumours to PBS-treated tumours (individual
622 tumour volume (CLD group)/ mean tumour volume (Con group)). Right: T-cell infiltration of
623 MC38-OVA tumours in macrophage-depleted mice treated with CLD. Of note, the apparent
624 increase of $CD8^+$ T cells in clodronate-treated mice is only relative and results from macrophage
625 depletion. Clodronate liposomes, 150 µl (7 mg/ml) every three days starting 2 days before
626 CLD. **g**, Left: Progression of MC38-OVA tumours in *Adra2a*-KO mice treated with CLD after
627 adoptive transfer (ACT) of wild-type bone-marrow-derived macrophages. Right: $CD8^+$ T-cell
628 infiltration of MC38-OVA tumours in *Adra2a*-KO mice treated with CLD after ACT of wild-
629 type bone-marrow-derived macrophages. CLD, i.p., 5 mg/kg daily. Clodronate liposomes, 150
630 µl every three days starting 2 days before CLD. Data (mean ± s.e.m) were pooled from at least
631 two independent experiments, with n>5 per group. P values determined by ordinary two-way
632 ANOVA (f-g), *t*-test (Unpaired, two-tailed) (columns, e-g). **** $p<0.0001$.

633

634
635

Materials and Methods

Mice

TiRP mice were created by crossing Ink4a/Arf$^{flox/flox}$ mice with mice carrying a transgenic construct controlled by the tyrosinase promoter and driving the expression of *H-Ras^{12V}* and *Trap1a*, which encodes a MAGE-type tumour antigen P1A; the promoter is separated from the coding region by a stop cassette made of a floxed self-deleting CreER[10]. Those mice were backcrossed to a B10.D2 background and bred to homozygosity. TCRP1A mice heterozygous for the H2L^{d}/P1A$_{35-43}$-specific TCR transgene were kept on the B10.D2;Rag-1$^{-/-}$ background[49]. NSG mice (strain NOD.Cg-*Prkdc^{scid} Il2rg^{tm1Wjl}/SzJ*), C57BL/6J mice and BALB/c mice were used in tumour transplantation experiments. *Adra2a*-KO mice (strain B6.129-*Adra2a $^{tm1Bkk/J}$*, #004367) were obtained from Jackson Laboratory (Bar Harbor, ME, USA) and genotyped as described[50], using the following primers (5'-GGTGACACTGACGCTGGTTT (forward), 5'-AAGGAGATGACAGCCGAGAT (reverse WT), 5'-CGAGATCCACTAGTTCTAGC (reverse KO)). *Adrb1/b2*-KO mice (strain *Adrb1^{tm1Bkk} Adrb2$^{tm1Bkk/J}$,* # 003810) were obtained from Jackson Laboratory (Bar Harbor, ME, USA), backcrossed with C57BL/6J mice and genotyped using the standard protocol provided by Jackson Laboratory. OT-I mice (C57BL/6-Tg(TcraTcrb)1100Mjb/Crl) and OT-II mice (C57BL/6-Tg(TcraTcrb)425Cbn/Crl) were obtained from Charles River. Ly5.1 Mice were obtained from Charles River. All mice used were age matched and were assigned randomly to experimental and control groups. Investigators were blinded to allocation during experiments. Female TiRP mice (10-18 weeks), NSG mice (8-14 weeks), C57BL/6J, BALB/c, *Adra2a*-KO, *Adrb1/b2*-KO mice (6-12 weeks) were used for experiments on antitumour effect *in vivo*. Female TCR-P1A, TCR-OT I, TCR-OT II mice (9-12 weeks) were used for CD8 T cell isolation. Female Ly5.1 mice (6-12 weeks) were used to differentiate macrophages *in vitro* for adoptive cell transfer. Female and male DBA/2 mice (6-12 weeks)

were used for CD8 and CD4 T cell isolation for *in vitro* assays. The sample size was chosen based on preliminary experiments and previously published results. All mice used in this study were produced under specific pathogen free (SPF) conditions at the animal facility of the de Duve Institute, housed at an ambient temperature around 21-23 C°, humidity of 40-60% and a light dark cycle of 12 hours. All the rules concerning animal welfare have been respected according to the 2010/63/EU Directive. All procedures were performed with the approval of the Animal Ethical Committee of UCLouvain university, with reference 2015/UCL/MD/14 and 2019/UCL/MD/019.

Cell lines

CT26, B16-F1, HEPA1-6, J558, 4T1, Renca, PC-3 were purchased from American Type Culture Collection (ATCC). The B16F10-OVA cell line was generated by transduction of B16F10 cells (ATCC) with lentivirus encoding chicken ovalbumin protein in the lab. E.G7-OVA cell line was kindly provided by Prof. J. Vanginderachter (VUB, Belgium). TS/A cell line was kindly provided by Prof. G. Prodi, (University of Bologna, Italy). LS411N cell line was kindly provided by Prof. N. Odartchenko (CHUV, Lausanne, Switzerland). T429.6 cell line was generated from the induced TiRP melanoma tumour model in the lab[11]. (PMID: 29123081). The MC38 cell line was kindly provided by M. Waldner (University of Erlangen, Germany). MC38-OVA cell line was generated by transduction of MC38 cells with lentivirus encoding chicken ovalbumin protein. SK-OV-3 cell line was purchased from Cell Line Service. TC-1 cell line was kindly provided by C. Gérard (GlaxoSmithKline Biologicals, Rixensart, Belgium). CMS5a cell line was obtained from the lab of H. Shiku (Mie University School of Medicine, Japan). All tumour cell lines were tested regularly for mycoplasma contamination using MycoAlert® Mycoplasma Detection Kit (#LT07-318, Lonza) and were verified to be negative before using for different assays and studies. All murine tumour cell lines were validated using the ATCC

686 STR profiling Cell Authentication Service. All human cell lines were validated using the Eu-
687 rofin Cell line Authentication Service by PCR-single-locus-technology.
688
689 **Cell culture**
690 L1210.P1A.B7-1 cells were cultured in Dulbecco's Modified Eagle Medium (DMEM)
691 (#31885023, Gibco, Thermo Fisher Scientific) supplemented with 10 % fetal bovine serum
692 (FBS) (#F7524, Sigma Life Science), penicillin (100 U/mL) and streptomycin (100 µg/mL).
693 Mouse TCRP1A and TCR-OT1 $CD8^+$ T cells were cultured in IMDM medium (#21980032,
694 Gibco, Thermo Fisher Scientific) supplemented with 10 % FBS (#F7524, Sigma Life Science),
695 penicillin (100 U/mL), streptomycin (100 µg/mL), a mix of amino acids (L-asparagine (0.24
696 mM), L-arginine (0.55 mM) and L-glutamine (1.5 mM)) and recombinant IL-2 (25 U/mL)
697 (PROLEUKIN, Novartis). Cells were maintained at 37 °C in an atmosphere containing 8 %
698 CO_2. CT26, B16F1, B16F10-OVA, MC38, MC38-OVA, Hepa 1-6, TC-1, J558, TS/A, CMS5a,
699 SK-OV-3, LS411N, PC-3 cells were cultured in IMDM medium (#21980032, Gibco, Thermo
700 Fisher Scientific) supplemented with 10 % FBS (#F7524, Sigma Life Science), penicillin (100
701 U/mL), streptomycin (100 µg/mL), a mix of amino acids (L-asparagine (0.24 mM), L-arginine
702 (0.55 mM) and L-glutamine (1.5 mM)). Renca cells were cultured in the same medium further
703 supplemented with 1 mM pyruvate (#11360070, Gibco, Thermo Fisher Scientific). E.G7-OVA
704 and 4T1 cells were cultured in RPMI medium (#52400025, Gibco, Thermo Fisher Scientific)
705 supplemented with 10 % FBS (#F7524, Sigma Life Science), penicillin (100 U/mL), strepto-
706 mycin (100 µg/mL), and a mix of amino acids (L-asparagine (0.24 mM), L-arginine (0.55 mM)
707 and L-glutamine (1.5 mM)). All cells were maintained at 37 °C in an atmosphere containing 8
708 % CO_2.
709
710

Drug administration

Mice received a daily intra-peritoneal injection of guanabenz (5 mg/kg), clonidine (5 mg/kg), guanfacine (2 mg/kg), yohimbine (5 mg/kg), phentolamine (5 mg/kg), propranolol (5mg/kg) or vehicle (PBS) from the day of randomization until the day of sacrifice. Of note, mice (particularly Balb/c mice) were strongly sedated after injection of α2-AR agonists, but they always fully recovered after 30-60 minutes. Likewise, α2-AR agonists increased the aggressiveness of male mice, therefore female mice were used for all experiments. For the co-administration of adrenergic receptor agonist and antagonist, mice received daily injections of vehicle control, guanabenz (5 mg/kg, i.p.) or guanabenz (5 mg/kg, i.p.) plus yohimbine (10 mg/kg, i.p.), clonidine (5 mg/kg, i.p.) or clonidine (5 mg/kg, i.p.) plus yohimbine (10 mg/kg, i.p.) when the tumour size was around 50 mm^3, until the day of sacrifice. When given in drinking water, clonidine was diluted in sterilized water at a concentration of 10 µg per ml.

The anti-CTLA4 (BioXcell, clone 9H10, 40 µg/mouse) and anti-PD-1 (BioXcell, clone RMP1-14, 200 µg/mouse) antibodies were injected twice per week i.p. starting 1 day before the α2-AR agonists injections. The anti-MHC II antibody (BioXcell, clone Y-3P, 500 µg/mouse) was injected twice per week i.p. starting 1 day before the α2-AR agonists injections. The corresponding isotype controls were injected accordingly (InVivoMAb rat IgG2b isotype control (#BE0090, BioXcell) InVivoMAb rat IgG2a isotype control (#BE0089, BioXcell), InVivoMAb polyclonal Syrian hamster IgG (#BE0087, BioXcell)). One day prior to the initiation of the therapy regimens, fingolimod (FTY720, Enzo Life Sciences) was given to mice to inhibit lymphocyte migration out of lymphoid organs. Mice received a dose of 10 µg FTY720 per mouse i.p. daily throughout the experiment.

MDSC suppression assay

After mechanical and enzymatic dissociation of induced TiRP tumours, Ly6G^{high} cells were further purified by magnetic sorting (Miltenyi) and confirmed as PMN-MDSC by FACS analysis (Gr-1^{high}, CD11b^{+}, Ly6C^{low} and Ly6G^{high}). TCRP1A CD8^{+} T cells activated *in vitro* for 4 days with irradiated (100 Gy) L1210.P1A.B7-1 cells were purified, washed, counted and 2×10^5 viable cells were seeded in a 96-well plate in IMDM complete medium. TCRP1A CD8^{+} T cells were co-cultured with Ly6G^{+} MDSCs at the indicated ratios for 2 days at 37 °C. T-cell apoptosis was assessed by Annexin V staining. T-cell number was counted by flow cytometry analysis using Precision count beads.

***In vitro* T-cell activity assay**

TCRP1A CD8^{+} T cells activated *in vitro* for 4 days with irradiated L1210.P1A.B7-1 cells were purified, washed, counted and 2×10^5 viable cells were seeded in a 96-well plate in IMDM complete medium. T-cell degranulation was induced by co-culturing the CD8^{+} T cells with L1210.P1A.B7-1 cells with and without clonidine. After 2 hours of co-culture, T-cell degranulation was measured by examination of Lamp1 expression. For assessing the Ifn-γ production, TCRP1A CD8^{+} T cells were co-cultured with L1210.P1A.B7-1 cells for 16 hours with and without clonidine, supernatant was collected and the amount of secreted Ifn-γ was quantified by ELISA according to manufactures instruction (#DY485, R&D systems). In parallel, T cells were also counted at the end of the 16-hour co-culture.

Tumour induction with 4-OH-Tamoxifen

A fresh solution of 4-OH-Tamoxifen was prepared by dissolving 4OH-Tamoxifen (Imaginechem®) in 100 % ethanol and mineral oil (ratio 1:9) followed by 30 min sonication, and

injected subcutaneously (2 mg/200 µL per mouse) in the neck area of gender-matched 7-week old TiRP mice.

Tumour transplantation

Different tumour cell lines were cultured at 37 °C in an atmosphere containing 8 % CO_2. Cells were collected and injected (1 million cells) subcutaneously into the right flank of the recipient mice.

Adoptive cell transfer of $CD8^+$ T cells

For the adoptive cell transfer (ACT), P1A-specific (TCRP1A) $CD8^+$ T cells or OVA-specific (TCROVA) $CD8^+$ T cells were isolated from spleens and lymph nodes of TCRP1A mice or OT-I mice, respectively. TCRP1A $CD8^+$ T cells were stimulated *in vitro* by co-culture with irradiated (100 Gy) L1210.P1A.B7-1 cells[51] at 1:2 ratio ($0.5x10^5$ $CD8^+$ T cells and 10^5 L1210.P1A.B7-1 cells per well in 48-well plates) in IMDM (GIBCO®) containing 10 % fetal bovine serum supplemented with L-arginine (0.55 mM, Merck®), L-asparagine (0.24 mM, Merck®), glutamine (1.5 mM, Merck®), beta-mercaptoethanol (50 µM, Sigma Aldrich®), 50 U/mL penicillin and 50 mg/mL streptomycin (Life Technologies®). TCROVA $CD8^+$ T cells were stimulated *in vitro* with Mouse T-Activator CD3/CD28 Dynabeads (#11453D, Gibco, Thermo Fisher Scientific) in 48-well plate (#3548, Corning Incorporated) at a ratio of 1 to 1 (100 000 TCROVA $CD8^+$ T cells mixed with 100 000 beads per well) in the presence of 25-unit interleukin 2. Four days after T cell activation, TCRP1A $CD8^+$ T cells were purified on a Lymphoprep gradient (StemCell®) and 10^7 living cells were injected intravenously in 200 µL PBS in TiRP-tumour bearing mice on the day of randomization. For TCROVA $CD8^+$ T cells, cells were collected 7 days after activation and 10^7 living cells were injected intravenously in 200 µL PBS in MC38-OVA tumour bearing mice.

Adoptive cell transfer with *in vitro* differentiated macrophages

Femora and tibiae of 8–10 weeks old C57BL/6J mice were flushed with DMEM medium. Bone marrow cells were cultured in DMEM medium containing 10 % FBS, 10 ng/ml MCSF, 50 U/mL penicillin and 50 mg/mL streptomycin (Life Technologies®) in the atmosphere of 37 °C, 5 % CO_2. Medium was refreshed on day 4. On day 7, medium was replaced by DMEM medium containing 10 ng/ml Ifn-γ, 10 % FBS, 10 ng/ml MCSF, 50 U/mL penicillin and 50 mg/mL streptomycin (Life Technologies®) to differentiate macrophages and the cells were further cultured for another three days. On day 10, differentiated macrophages were detached from culture flask using Accutase (#00-4555-56, Gibco, Thermo Fisher Scientific), resuspended in PBS and transferred to recipient mice by intravenous injection (2×10^6 cells per mouse) when tumour size reached around 100 mm^3. Mice then received daily clonidine treatment (i.p., 5 mg/kg) starting 1 day after macrophage transfer. In the experiment where $CD45.1^+$ macrophages were used for adoptive cell transfer, bone marrow cells from Ly5.1 C57BL/6J congenic mice expressing the CD45.1 allele were used for macrophage differentiation.

Tumour growth measurement

The size of individual tumours was measured every two or three days. The tumour diameters (width, length) were measured with digital caliper. Tumour volumes were calculated using the formula: volume = ($width^2$ x length) /2. Tumour measurement was recorded and calculated by Microsoft Excel for Mac (16.7).

Isolation of human peripheral blood mononuclear cells (PBMCs)

PBMCs were derived from the blood of different hemochromatosis patients, courtesy of Saint-Luc University Hospital. They were isolated by centrifugation on a Lymphoprep gradient and

were used freshly for adoptive cell transfer. The study protocol was approved by "UCLouvain commission d'éthique hospitalo-facultaire" under authorisation approval n° CEHF 2021/13SEP/373. The ethical approval encompasses an exemption of informed consent based on the fact that we only use blood that qualifies as “Residual Human Body Material”, which needs to be collected as a therapeutic measure for hemochromatosis patients. The absence of “opting out” option was checked for all patients.

Human xenografts in NSG mice reconstituted with human lymphocytes

NSG mice (from The Jackson Laboratory) were bred at the animal facility of the de Duve Institute, Brussels, Belgium. Handling of mice and experimental procedures were conducted in accordance with national and institutional guidelines for animal care. NSG mice were injected subcutaneously with 1.5×10^6 SK-OV-3, LS411N or PC-3 cells. After tumour appearance, tumours were measured, mice were randomized based on tumour size and injected or not with 3×10^6 human allogeneic PBMCs (PBMC; d0) intravenously. Guanabenz or clonidine (5 mg/kg) was injected i.p. daily. Tumours were measured at regular intervals with an electronic caliper.

Single-cell preparation for FACS staining

Tumours and spleens were isolated from tumour-bearing mice. Tumour samples were dissociated by using a cocktail of three enzymes (Collagenase I, Collagenase II and Dispase) with the help of a gentleMACS dissociator (Miltenyi). Spleens were gently smashed in cell culture medium to generate a cell suspension. Single cells were obtained by filtration of tissue homogenate through a 40-µm filter.

Generation of *Adra2a*-KO tumour cells

TC-1 tumour cells were electroporated with Cas9/gRNA RNP targeting *Adra2a* (#Mm. Cas9.ADRA2A.1AA, # Mm. Cas9.ADRA2A.1AB, IDT). Cells were resuspended in SE Cell Line 4D-Nucleofector X Kit solution with supplement (Lonza), transferred to 16-well Nucleocuvette strips and electroporated using program DS-120. One week after electroporation, single cell clones were isolated by Facs sorting (MA900 Multi-Application Cell Sorter) and were expanded and validated by RT-qPCR analysis.

CFSE tumour proliferation assay

Carboxyfluorescein diacetate succinimidyl ester (CFDA-SE Cat# C1157, Molecular Probes, USA) stock solution (5 mM) was dissolved in DMSO. 2×10^7 tumour cells in 10 ml IMDM medium without serum were mixed with 2.5 μM CFDA-SE, and the cell/CFDA-SE mixture was incubated at 37 °C for 10 min. The labeling reaction was stopped by incubation with full IMDM medium containing serum. The CFSE-labeled cells were washed twice with IMDM medium containing 10 % FBS and recounted, then used for proliferation assesment. The CFSE fluorescence intensity was measured by flow cytometry analysis.

MTT assay

Tumour cells ($1.5x10^3$) were plated in triplicate in a 96-well plate in a cell-cell direct contact manner with 0.1 ml complete medium containing different α2-AR agonists at different concentrations. 48 hours after treatment, cell viability was measured using MTT [3-(4,5-dimethylthiazol-2-yl)-2,5-diphenyltetrazolium bromide] assay.

Western blot analysis

Cell lysates were added with Pierce Lane Marker Reducing Sample Buffer (ThermoFisher, #39000), heated (95°C, 10min) and loaded on polyacrylamide gel (Bolt 4-12 %, Invitrogen,

#NW04122). After migration, proteins were transferred to iBlot NC stacks (Invitrogen, #IB23002). Membrane was blocked with 5 % BSA and stained with anti- Phospho-CREB (Ser133) antibody (Cell Signaling, clone 87G3, #9198, 1:1000), CREB antibody (Cell signaling, clone 48H2, #9197, 1:1000), or anti-beta actin antibody (Cell Signaling, clone 13E5, #5125, 1:1000). Secondary antibodies used were anti-rabbit IgG HRP (Cell signaling, #7074, 1:2500). Protein detection was performed with the chemiluminescent SuperSignal WestPico substrate (ThermoScientific, #34578). Pictures were captured with Fusion FX camera (Vilbert Lourmat).

Macrophage co-culture assay.

M1 Macrophages were differentiated *in vitro* as described above. For co-culture experiments with allogeneic T cells, 3 x 10^4 naïve mouse $CD4^+$ and/or $CD8^+$ T cells were co-cultured with 5 x 10^4 allogeneic M1 macrophages per 200 µl in round-bottomed 96-well culture plates in the presence of the indicated concentrations of clonidine. Four days after co-culture, T cell numbers were recorded by flow cytometry analysis using Precision count beads.

For co-culture experiments with syngeneic OT-I $CD8^+$ T cells and OT-II $CD4^+$ T cells, 3 x 10^4 CFSE labeled naïve mouse $CD4^+$ and/or $CD8^+$ T cells were co-cultured with 5 x 10^4 M1 macrophages with or without 2.5 µM clonidine in presence of 1 µg/ml ovalbumin protein (InvivoGen, #vac-pova-25) per 200 µl in round-bottomed 96-well culture plates in the presence of 2.5 µM of clonidine. To assess the role of MHC II, anti-MHC II antibody (50 µg/ml) was added in the co-culture as indicated. Three days after co-culture, T-cell proliferation index was analyzed by flow cytometry analysis using the function of proliferation modeling. Ifn-γ production was assessed in OT-I $CD8^+$ T cells co-cultured as above and stimulated with 3 x 10^4 E.G7-OVA tumour cells for 16 hours. Intracellular Ifn-γ was measured by flow cytometry.

cAMP quantification.

In vitro differentiated M1 macrophages were treated with different concentration of clonidine. Cyclic AMP Competitive ELISA Kit was used to assay cAMP (#EMSCAMPL, Thermo fisher).

FACS staining of tumour-infiltrating immune cells

Single cell suspension from tumours and spleens of tumour-bearing mice were counted and plated in round-bottom 96-well plate (#353910, FALCON), at a density of 10^6 cells per well. Cells were blocked with Mouse TruStain FcX™ and were stained with viability dye Efluor™ 780 (#65-0865-14, Invitrogen, 1 in 500 dilution in PBS) to identify living cells, followed by staining with P1A-tetramer (home-made H-2-L^d folded with P1A peptide LPYLGWLVF; 1 in 50 dilution) and anti-CD45, anti-CD8 antibody to identify tumour-infiltrating $CD8^+$ T cells. The apoptosis of T cells was analyzed using Annexin V-APC. Ly6C-PerCP, Gr-1-APC, Ly6G-Bv510, CD11b-Bv711 antibodies were used to identify MDSCs. F4/80-PE, MHC class II-APC (1:500), CD11c-Bv421 antibodies were used to identify macrophages. PD-1-FITC, PD-L1-PE, Ifn-γ-APC, Tnf-α-Bv711 were used to evaluate the expression of different immune modulators by cells of the TME. All antibodies are used with a dilution of 1:200 unless specified. For intracellular staining, cells were fixed using Fixation Buffer (Biolegend, #420801,) and permeabilized with Perm/wash Permeabilization Buffer (BioLegend, #421002). Antibodies were purchased from Biolegend and the concentration of antibodies used were according to manufacturer's recommendation. Phagocytosis of macrophages was measured by using pHrodo™ Red E. coli BioParticles™ Conjugates for Phagocytosis (Thermo Fisher) according to the manufacturer's recommendation. Flow cytometry data were analyzed by Flowjo version 10.7.2.

In vivo depletion of $CD8^+$ or $CD4^+$ T cells

For CD8 T cell depletion, mice were given 500 µg of mAb 53-6.7 (BioXCell) or normal rat IgG (controls) by the i.p. route 1 day before starting clonidine treatment, and then 150 µg weekly. For CD4 T cell depletion, mice were given 500 µg of Ultra-LEAF™ Purified anti-mouse CD4 Antibody (Clone GK1.5, Biolegend) or normal rat IgG2b (controls) by the i.p. route 1 day before starting clonidine treatment, and then 250 µg weekly. Depletion was checked by FACS at the end of the experiment.

In vivo depletion of macrophages

Clodronate liposomes and control liposomes were purchased from FormuMax Scientific (Sunnyvale, CA, USA), and were injected (150 µL of 7 mg/ml) intraperitoneally 48 h before starting clonidine treatment, and repeated every 3 days till the end of the experiment. Depletion was checked by FACS at the end of the experiment.

Quantitative RT-qPCR

NucleoSpin RNA XS isolation kit (Macherey-Nagel) or NucleoSpin RNA isolation kit (Macherey-Nagel) was used to extract total RNA from cell lines or tumour tissues, respectively. RNA concentration was measured using NanoDrop 2000c (Thermo Scientific). Reverse transcription was performed using RevertAid RT kit (#K1691, Thermo Scientific). Quantitative PCR reactions were performed with primers and probes specific for murine *Adra2a* (Mm.PT.58.33590743.g), *Adra2b* (Mm.PT.58.6098909.g), *Adra2c* (Mm.PT.58.30363072.g), *Ifnb1* (Mm.PT.58.30132453.g), *Cxcl13* (Mm.PT.58.31389616), *Tlr1* (Mm.PT.58.45864869), *Tlr8* (Mm.PT.58.16021150), *Tlr7* (Mm.PT.58.10526075), *Gapdh* (Mm.PT.39a.1) (housekeeping gene), and for human *ADRA2A* (Hs.PT.56a.878688.g), *ADRA2B* (Hs.PT.58.723437.g), and

GAPDH (Hs.PT.39a.22214836) (housekeeping gene), using Takyon ROX Probe 2X MasterMix dTTP Blue (#UF-RPMT-B0701, Eurogentec) qPCR kit, and analysed on Applied Biosystems StepOnePlus Real-Time PCR System (#4376599, Thermo Fisher Scientific). All primers and probes were purchased from Integrated DNA Technologies. cDNA was amplified as followed: 45 cycles of a two-step PCR program at 95 °C for 3 s and 60 °C for 30 s. All determinations were performed in duplicates.

RNA sequencing sample preparation

Total RNA was extracted from 3 PBS-treated MC38-OVA tumours, 3 clonidine and 3 guanabenz-treated MC38-OVA tumours from wild-type mice or *Adra2a*-KO mice, 7 days after the starting of the treatment. Tumour tissue was collected and snap-frozen in liquid nitrogen. RNA extraction was initiated by grinding the tissue under liquid nitrogen into powder and further processed by using NucleoSpin RNA isolation kit (Macherey-Nagel). RNA quality was assessed by Agilent 2100 Bioanalyzer System. RNA samples with an RNA integrity number (RIN) above 7 were further used for RNA sequencing. Strand-specific mRNA-seq libraries for the Illumina platform were generated and sequenced at Genewiz (BaseClear, Leiden, The Netherlands). Libraries were multiplexed, clustered, and sequenced on an Illumina NovaSeq 6000, paired end, 150bp reads.

RNA sequencing downstream analysis

Quality control and filtering followed the trim galore! 0.6.5 protocol, which uses FastQC for quality control and Cutadapt for adapter trimming. Processed paired FASTQ files were mapped to the mouse reference GRCm38(Ensembl 96) and quantified with Kallisto 0.46.1 [52] on Ubuntu 20.04.1. The resulting transcript abundance matrices (estimated counts) per sample were subsequently imported with tximport[53] 1.20.0 in R version 4.0.3, summarized to gene level with

TxDB 3.10 annotations and finally submitted for differential expression analysis with DESeq2[54] 1.32.0. Effect sizes for comparison between treated and untreated conditions were estimated using apeglm as implemented in DESeq2.

Gene-level expression data generated in this study for each of the conditions was L1-normalised per sample using scikit-learn 0.24.1 (https://jmlr.csail.mit.edu/papers/v12/pedregosa11a.html). Signature correlations between all samples were calculated as Spearman correlations (SciPy 1.6.2) using only the genes in the α2-AR activation signature. The resulting distance matrix was then projected on top of a manifold using UMAP-learn 0.5.1 [55]. Hierarchical clustering (SciPy 1.6.2) using Spearman correlation on the expression matrix of the α2-AR activation signature genes, identified 3 broad clusters separating KO and unstimulated conditions from the stimulated wild-type samples, highlighted in Extended Data Fig. 4h with ellipses.

TCGA-based validation

Gene expression data and immune features associated with TCGA, as calculated by Thorsson [56] and co-workers was downloaded from the corresponding GDC portal at https://gdc.cancer.gov/about-data/publications/panimmune (n = 10496, 33 cancer types). H&E-derived metrics [57] for $CD8^+$ T cell infiltration were also obtained from the GDC (https://gdc.cancer.gov/about-data/publications/tilmap). Correlations between expression of a selected set of immune modulators and the ADRA2 metagene (sum of *ADRA2A, ADRA2B, ADRA2C*) were calculated using Spearman correlations with SciPy 1.6.2[58]. Heatmaps and boxplots were plotted with Python 3.8.8, through matplotlib 3.5.2[59] and seaborn 0.11.1[60]. Kaplan-Meier curves based on gene expression were generated with lifelines 0.26.3, using the median gene expression as threshold between groups.

TIDE survival analysis

To test survival impact of the up- and downregulation signatures, we consulted the TIDE[61] database through its web portal (http://tide.dfci.harvard.edu/login/). Gene signatures were entered as biomarker and tested for survival impact. Kaplan-Meier curves were calculated using the median value of the signature metagene to discriminate between "high" and "low" expression. Statistical significance was tested with a two-sided Wald's test in a (Cox Proportional Hazards) CoxPH regression model.

Sample preparation for single-cell sequencing

MC38-OVA tumour samples isolated from mice treated with PBS or Clonidine (7 days after starting of the treatment) were pooled (10 mice per group) and dissociated using a cocktail of three enzymes (Collagenase I, Collagenase II and Dispase) with the help of a gentleMACS dissociator (Miltenyi). The cell suspension was collected, filtered through a 70-µm filter (#352350, FALCON) and washed with cold sterile phosphate-buffered saline (PBS). Dead cell removal was performed using Ficoll gradient. Briefly, cell pellets were resuspended in 10 ml PBS and gently layered on top of 10 ml the density gradient medium (Lymphoprep) followed by a centrifugation at 3000 rpm for 10 minutes at room temperature with the brake off. Cells were collected at the interface and prepared for single-cell sequencing as described by the manufacturer (10X Genomics) in "Methanol fixation of cells for single-cell RNA sequencing protocol". Single-cell mRNA sequencing was performed at Single Cell Discoveries (single-cell sequencing service, the Netherlands) according to standard 10x Genomics 3' V3.1 chemistry. Prior to loading the cells on the 10x Chromium controller, cells were rehydrated in rehydration buffer following vendor instructions. Cells were then filtered to prevent clumping and counted to assess cell integrity and concentration. Cells were loaded and the resulting sequencing libraries were

prepared following standard 10x Genomics protocol. The DNA libraries was paired-end sequenced on an Illumina Novaseq S4, with a 2x150 bp Illumina kit. BCL files resulting from sequencing were transformed to FASTQ files with 10x Genomics Cell Ranger version 6.1.2 mkfastq. FASTQ files were mapped with Cell Ranger count. During sequencing, Read 1 was assigned 28 base pairs, and was used for identification of the Illumina library barcode, cell barcode and UMI. R2 was used to map to the reference transcriptome mm10 2020A. Filtering of empty barcodes was done with Cell Ranger. Unsupervised clustering and differential gene expression analysis was done with the Seurat1 R toolkit[62] version 4.0.3. For TC-1 tumours, sample preparation was performed the same way as described above, except fresh cells were directly loaded, and the resulting sequencing libraries were prepared following the standard 10x Genomics protocol.

scRNAseq analyses

10X files generated by CellRanger version 6.1.2 were loaded into Scanpy[63] 1.7.0 and quality control metrics were calculated. Cells with either low (<200) or higher than expected (>2,500) number of individual genes expressed were removed. Genes with very limited expression (less than 10 cells) were removed. Counts were normalized per 10,000 reads and log2-transformed. Differences in total counts per cell and mitochondrial content were regressed out. Highly variable genes were detected using the Seurat approach, with a mean expression cut-off of 0.125. Only highly variable genes were used for PCA, clustering and downstream set enrichment analysis. We clustered MC38-OVA cells into groups with PhenoGraph version 1.5.7[64] (https://github.com/dpeerlab/phenograph), using the Leiden clustering algorithm. The parameters were k=25, 5000 iterations and random seed 770. The number of PCA components we selected explained 20 % of the total variance in the dataset (n_comps=26). MC38-OVA cell

populations were manually annotated per cluster, based on known marker genes (Supplementary file 1). In total, 12,066 MC38-OVA cells passed quality control filtering. 2,213 genes were identified as highly variable. Differential expression testing between treated and untreated was performed using Wilcoxon rank sum tests with α=0.05, using Diffxpy 0.7.4. Analysis of ligand-receptor interactions between cells in the sample was performed with CellPhoneDB[65] v2.1.4. To this end, mouse genes were mapped to their human orthologs using BioMart (Ensembl release 104).

10X files generated by CellRanger for the TC-1 lung carcinoma validation set were loaded into R 4.2.0 Patched (2022-05-13 r82357) using the read10xCounts() function from the DropletUtils[66] package version 1.16.0. Quality metrics were computed using the scuttle package[67] version 1.6.3 and cells with over 10% of mitochondrial gene counts were removed. Counts where then normalised by deconvolution using the scran package[68] version 1.24.1, and the 1,000 most variable genes were selected based on their per-gene variance as implemented in scran. 19,069 cells and the 1,000 most variable genes were used for downstream clustering and cell annotations. Clusters were identified using scran's clusterCells() function applying a two-step procedure, starting with a vector quantisation with k-means on the PCA-reduced data (200 centres and 100 iterations) to obtain representative centroids that are then subjected to nearest-neighbour graph-based clustering as described above, using k = 10 nearest neighbours. Cell type annotation was performed using the SingleR package version 1.10.0 as above, using the MC38-OVA colon carcinoma single cell data annotations described above.

Set enrichment analysis

For both RNAseq and scRNAseq data, genes were pre-ranked based on log2 fold change and processed with GSEApy version 0.10.5 (https://pypi.org/project/gseapy/), which implements

the classical GSEA[69] analysis. Gene sets for mouse enrichment were obtained from http://baderlab.org/GeneSets on 11/02/2021.

Statistics

Statistical significance was assessed by two-sided unpaired Welch *t*-test unless otherwise specified. The *P* values are annotated as follows: *, $P < 0.05$; **, $P < 0.01$; ***, $P < 0.005$; and ****, $P < 0.0001$. For the mouse *in vivo* experiments, statistical significance was determined using two-way ANOVA to compare differences among multiple groups. All statistical analyses were performed using GraphPad Prism version 8.4.3 for Mac (GraphPad Software, San Diego, CA, USA, www.graphpad.com), R 4.0.3 (for RNAseq analysis), and R 4.2.0 (for scRNAseq analysis), and Python 3.7.3 (for the RNAseq and scRNA-seq data analysis) and Python 3.8.8 (for data visualization).

Data and code availability statement

The authors declare that all other data supporting the findings of this study are available within the article and its supplementary information files. scRNAseq and RNAseq were obtained from in-house experiments. Raw and processed data are available from GEO under accessions GSE227601 and GSE226290 respectively. Supporting R and Python scripts, with installation instructions and version numbers are publicly available on GitHub at https://github.com/BVDElab/Tumour_immune_rejection and archived on Zenodo under DOI: 10.5281/zenodo.7751788 (https://doi.org/10.5281/zenodo.7751788). Code to generate supplementary figures is available on Zenodo under DOI: 10.5281/zenodo. 7789646 (https://doi.org/10.5281/zenodo.7789646).

Acknowledgements

We thank Isabelle Grisse for editorial assistance, Pedro Gomez for large-scale production of different mouse strains, and Pierre Coulie for critical comments. Minh-Phuong Le, and Matteo Formenti for excellent technical assistance. J. Z was supported by Fondation Contre le Cancer (Grant number 2019-094). This work was supported by WELBIO (Walloon Excellence in Life Sciences and Biotechnology), Belgium(Grant WELBIO-CR-2019C-05); Fonds pour la Recherche Scientifique (FNRS), Belgium (Grants EOS O000518F and PDR T.0091.18); Fondation contre le Cancer, Belgium (Grant 2018-090). Ludwig Cancer Research, and de Duve Institute. The results shown here are in whole or part based upon data generated by the TCGA Research Network: https://www.cancer.gov/tcga.

Author contributions

J.Z. conceived the project and analysed the data. J.Z. and L.B. performed all the *in vivo* experiments. L.B. performed the *in vitro* experiments. S.N. analyzed the single cell sequencing and bulk RNA sequencing data for the MC38-OVA tumour model, L.G. and M.M. analyzed the single cell sequencing data for the TC-1 tumour model. B.J.V.d.E. helped to conceive and design experiments, analysis data and interpret results. J.Z. and B.J.V.d.E. wrote the manuscript. All authors were involved in the data interpretation and manuscript preparation. .

Competing interest declaration

J.Z and B.J.V.d.E are inventors on patent applications related to using alpha2-adrenergic receptor agonists in cancer immunotherapy. The other authors have no competing interests.

Additional information

Supplementary information is available for this paper at

Correspondence and requests for materials should be addressed to Jingjing Zhu.

Reprints and permissions information is available at www.nature.com/reprints.

References:

49 Shanker, A. *et al.* Thymocyte-intrinsic genetic factors influence CD8 T cell lineage commitment and affect selection of a tumor-reactive TCR. *J. Immunol.* **172**, 5069-5077 (2004).

50 Ohshima, M., Itami, C. & Kimura, F. The alpha2A -adrenoceptor suppresses excitatory synaptic transmission to both excitatory and inhibitory neurons in layer 4 barrel cortex. *J Physiol* **595**, 6923-6937, doi:10.1113/JP275142 (2017).

51 Gajewski, T. F., Renauld, J. C., Van Pel, A. & Boon, T. Costimulation with B7-1, IL-6, and IL-12 is sufficient for primary generation of murine antitumor cytolytic T lymphocytes in vitro. *J Immunol* **154**, 5637-5648 (1995).

52 Bray, N. L., Pimentel, H., Melsted, P. & Pachter, L. Near-optimal probabilistic RNA-seq quantification. *Nat. Biotechnol.* **34**, 525-527, doi:10.1038/nbt.3519 (2016).

53 Soneson, C., Love, M. I. & Robinson, M. D. Differential analyses for RNA-seq: transcript-level estimates improve gene-level inferences. *F1000Res* **4**, 1521, doi:10.12688/f1000research.7563.2 (2015).

54 Love, M. I., Huber, W. & Anders, S. Moderated estimation of fold change and dispersion for RNA-seq data with DESeq2. *Genome biology* **15**, 550, doi:10.1186/s13059-014-0550-8 (2014).

55 Sainburg, T., McInnes, L. & Gentner, T. Q. Parametric UMAP Embeddings for Representation and Semisupervised Learning. *Neural. Comput.* **33**, 2881-2907, doi:10.1162/neco_a_01434 (2021).

56 Thorsson, V. *et al.* The Immune Landscape of Cancer. *Immunity* **48**, 812-830 e814, doi:10.1016/j.immuni.2018.03.023 (2018).

57 Saltz, J. *et al.* Spatial Organization and Molecular Correlation of Tumor-Infiltrating Lymphocytes Using Deep Learning on Pathology Images. *Cell reports* **23**, 181-193 e187, doi:10.1016/j.celrep.2018.03.086 (2018).

58 Virtanen, P. *et al.* SciPy 1.0: fundamental algorithms for scientific computing in Python. *Nat Methods* **17**, 261-272, doi:10.1038/s41592-019-0686-2 (2020).

59 Hunter, J. D. Matplotlib: A 2D Graphics Environment. *Comput Sci Eng* . **9**, 90-95, doi:doi:10.1109/MCSE.2007.55 (2007) (2007).

60 Waskom, M. L. seaborn: statistical data visualization. *J. Open Source Softw.* **6**, 3021, doi:doi:https://doi.org/10.21105/joss.03021 (2021).

61 Jiang, P. *et al.* Signatures of T cell dysfunction and exclusion predict cancer immunotherapy response. *Nat Med* **24**, 1550-1558, doi:10.1038/s41591-018-0136-1 (2018).

62 Butler, A., Hoffman, P., Smibert, P., Papalexi, E. & Satija, R. Integrating single-cell transcriptomic data across different conditions, technologies, and species. *Nature biotechnology* **36**, 411-420, doi:10.1038/nbt.4096 (2018).

63 Wolf, F. A., Angerer, P. & Theis, F. J. SCANPY: large-scale single-cell gene expression data analysis. *Genome biology* **19**, 15, doi:10.1186/s13059-017-1382-0 (2018).

64 Levine, J. H. *et al.* Data-Driven Phenotypic Dissection of AML Reveals Progenitor-like Cells that Correlate with Prognosis. *Cell* **162**, 184-197, doi:10.1016/j.cell.2015.05.047 (2015).
65 Efremova, M., Vento-Tormo, M., Teichmann, S. A. & Vento-Tormo, R. CellPhoneDB: inferring cell-cell communication from combined expression of multi-subunit ligand-receptor complexes. *Nat Protoc* **15**, 1484-1506, doi:10.1038/s41596-020-0292-x (2020).
66 Griffiths, J. A., Richard, A. C., Bach, K., Lun, A. T. L. & Marioni, J. C. Detection and removal of barcode swapping in single-cell RNA-seq data. *Nat. Commun.* **9**, 2667, doi:10.1038/s41467-018-05083-x (2018).
67 McCarthy, D. J., Campbell, K. R., Lun, A. T. & Wills, Q. F. Scater: pre-processing, quality control, normalization and visualization of single-cell RNA-seq data in R. *Bioinformatics* **33**, 1179-1186, doi:10.1093/bioinformatics/btw777 (2017).
68 Lun, A. T., McCarthy, D. J. & Marioni, J. C. A step-by-step workflow for low-level analysis of single-cell RNA-seq data with Bioconductor. *F1000Res.* **5**, 2122, doi:10.12688/f1000research.9501.2 (2016).
69 Subramanian, A. *et al.* Gene set enrichment analysis: a knowledge-based approach for interpreting genome-wide expression profiles. *Proc Natl Acad Sci U S A* **102**, 15545-15550, doi:10.1073/pnas.0506580102 (2005).

Extended Data Figure legends

Extended Data Fig 1: Anti-tumour effects of clonidine and guanabenz in multiple tumour models. a, Survival curves of mice bearing MC38 colon carcinomas, B16F1 or B16F10 melanomas treated with CLD, GBZ, or vehicle. **b,** Progression of colon carcinomas MC38-OVA in mice treated with different doses of CLD. **c,** Anti-tumour effects of α2-AR agonists as monotherapy in multiple tumour models. GBZ or CLD was given daily (a, c: 5 mg/kg i.p.) starting at day 0 when tumours reached the indicated size. **d,** Progression of melanomas B16F10-OVA in C57BL/6J (immunocompetent) or NSG mice (immunodeficient) treated with vehicle (Con), GBZ or GFC. Data from one representative experiment out of two performed. GBZ (5 mg/kg) or GFC (2 mg/kg) was given daily (i.p.) starting 7 days after tumour implantation (day 0 = start of treatment). **e,** Progression of induced TiRP melanomas in mice treated with vehicle or GBZ. Left: mean growth curve; Right: individual growth curves. GBZ (5 mg/kg) was given daily (i.p.) starting at day 0 when tumours reached around 100 mm^3. The number of mice per group is indicated in brackets. Data (mean ± s.e.m) from one representative experiment out of three (e). P values determined by: ordinary two-way ANOVA (b-e), Log-rank (Mantel-Cox) test was used for the statistical evaluation of survival (a), $p<0.0001$.

Extended Data Fig 2: *Adra2a*, *Adra2b* and *Adra2c* expression in murine tumour cell lines (a), effect of agonists on tumour cell lines *in vitro* (b, c), and gating strategy for flow cytometry analysis of TME cells (d).

a, Expression of *Adra2a*, *Adra2b* and *Adra2c* in murine tumour cell lines was measured by RT-qPCR. **b,** Effect of α2-AR agonists on cell viability of different tumour cell lines. Cells were treated with different concentrations of GBZ, CLD or GFC for 48 hours and cell viability was measured by MTT assay. **c,** Effect of α2-AR agonists on cell proliferation of different tumour cell lines. CFSE assay was used to measure proliferation. During each round of cell division, intracellular CFSE

becomes diluted and is quantified (Median fluorescence intensity (MFI) of CFSE) to determine proliferation rate. **d,** Gating strategy on tumour samples for tumour-infiltrating $CD8^+$ T cells (Fig. 1b,d, 2b, 3e,g, 4f,g, Extended Data Fig. 4b,c, 7c), MDSCs (PMN-MDSC: $CD11b^+$ Gr-1^{high}, $Ly6C^{low}$, $Ly6G^{high}$, M-MDSC:$CD11b^+$ Gr-1^{low}, $Ly6C^{high}$, $Ly6G^{low}$) (Fig. 3g, Extended Data Fig. 4c,f, 6f) and macrophages ($CD11b^+$, $F4/80^+$) (Fig. 4e, Extended Data Fig. 6b,c,d,e, 8a,c, 10a). **e,** Gating strategy for Extended Data Fig. 6g. **f,** Gating strategy for Fig. 3g. **g,** Gating strategy for Fig. 3d, Extended Data Fig. 6j. **h,** Gating strategy for Extended Data Fig. 6i. Data (mean ± s.e.m, technical duplicates for a and c, technical sextuplicate for b) from one representative out of two independent experiments.

Extended Data Fig 3: Effect of α2-AR agonists on human tumour xenografts in humanized models (a-c), combination of α2-AR agonists with ICB (d-h), and gentoyping of *Adra2a*-KO mice (ij).

a-b, Progression of human xenografts of colorectal carcinomas LS411N (a) or prostate carcinomas PC-3 (b) in NSG mice (immunodeficient) treated with vehicle, GBZ or CLD after adoptive transfer of allogeneic human PBMC. Human PBMC were injected (i.v.) on day 0 when tumours reached the indicated size. Treatments (5 mg/kg daily i.p.) started on the same day. Mean ± s.e.m from one representative out of two independent experiments. **c,** Expression of *ADRA2A* and *ADRA2B* in human tumour cell lines measured by RT-qPCR. Data from one representative out of two independent experiments. **d,** Survival of MC38-OVA tumour-bearing mice treated with GBZ, CLD and/or anti-PD-1, as indicated. **e,** Individual tumour growth curves for mice from (d) **(**CR: complete tumour rejection). **f,** Survival of TC-1 tumour-bearing mice treated with CLD, anti-PD-1 or both. **g**, Progression of colon carcinomas CT26 in mice treated with GBZ, anti-PD-1, anti-CTLA4, or combinations of these. Treatments started on day 0 (7 days after tumour implantation). **h,** Progression of melanomas B16F1 in mice treated with CLD, anti-PD-1, or both. CLD

and GBZ were given daily (5 mg/kg i.p.) starting at day 0 when tumours reached the indicated size. Anti-CTLA4 (40 µg) and anti-PD-1 (200 µg) antibodies (i.p.) were given 1 day before the first injection of α2-AR agonists, then twice a week. **i,** Expression of *Adra2a*, *Adra2b* and *Adra2c* measured by RT-qPCR in bulk tissue from MC38, B16F10-OVA and CT26 tumours. Each dot represents an individual mouse. **j,** Genotyping of *Adra2a*-KO mice. Genotyping was performed by PCR on genomic DNA from mouse tails, using primers described in the materials and methods. Mice with only the mutant band detected are identified as *Adra2a*-KO mice. Shown is the genotyping result for one batch of mice. Genotyping was repeated for all mice used. For gel source data, see Supplementary Figure 1a. Mean ± s.e.m. P values determined by: ordinary two-way ANOVA (a,b,g,h), Log-rank (Mantel-Cox) test was used for the statistical evaluation of mouse survival (d and f), **** $p<0.0001$.

Extended Data Fig 4: Effect of clonidine on T cells and myeloid cells (a-f), and transciptomic analysis of treated tumours (g-h).

a, Effect of CLD on TCRP1A $CD8^+$ T-cell proliferation *in vitro* (left panel) and activity as measured by T-cell degranulation (middle panel) and Ifn-γ ELISA (right panel). **b,** $CD4^+$ and $CD8^+$ T-cell infiltration in tumours, lymph nodes and spleens of MC38-OVA tumour-bearing mice analyzed by flow cytometry after 7 days of treatment with vehicle (n=14) or CLD (n=15). CLD was given daily by i.p. injections (5 mg/kg) starting when tumours reached 50 mm^3, and T-cell analysis was performed 7 days later. **c,** Progression, $CD8^+$ T-cell infiltration and PMN-MDSC infiltration/apoptosis, of induced TiRP melanomas in TiRP mice treated with CLD or GFC after ACT of 10 million activated TCRP1A $CD8^+$ T cells. **d,** GBZ and CLD induce apoptosis of PMN-MDSC *in vitro*. PMN-MDSCs were isolated from induced TiRP melanomas using MDSC isolation kit (Miltenyi biotec) and were cultured and treated with GBZ or CLD for 24 hours. Apoptosis was analysed by flow cytometry using Annexin V. **Left**: technical duplicate from one representative experiment out

of two independent experiments**; Right:** Data (mean ± s.e.m) of technical duplicates/triplicates pooled from MDSCs isolated from 4 different batches of mice. **e,** T-cell suppressive activity of $Ly6G^+$ myeloid cells (PMN-MDSC) isolated from induced TiRP melanomas, as measured by T-cell apoptosis (left) and T-cell number after co-culture (right). Technical duplicates from one representative experiment out of two. **f,** PMN-MDSC infiltration and $CD8^+$ T-cell apoptosis in MC38 tumours from wild-type or *Adra2a*-KO mice treated with vehicle, GBZ or CLD. CLD, GBZ (5 mg/kg) and GFC (2 mg/kg) were given daily (i.p.), starting on day 0 when tumours reached the indicated size. Tumours were analysed *ex vivo* on day 6. **g,** RT-qPCR confirmation of mRNA expression of selected genes identified in the RNA-seq analysis. Mean fold change relative to untreated wild-type mice ± s.e.m. for MC38-OVA tumours from wild-type or *Adra2a*-KO mice treated with CLD and GBZ, as explained in f. Mean ± s.e.m, n= 4 independent biological samples. **h,** UMAP projection of L1-normalised gene expression using the genes of the upregulated (Post_Up) and the downregulated (Post_Down) signatures as defined in Supplementary Table 2, highlighting differences between MC38-OVA tumours from wild-type and *Adra2a*-KO mice treated with CLD or GBZ, as compared to untreated tumours (6 conditions, n=3 per group). Clusters were identified with hierarchical clustering, using Spearman correlations between the samples as distance measure. Data (mean ± s.e.m) from one representative experiment out of two independent experiments (a-f). P values determined by: ordinary two-way ANOVA (c), *t*-test (Unpaired, two-tailed) (columns,a,b,c,d,f), **** $p<0.0001$.

Extended Data Fig 5: Single-cell RNAseq analysis of tumours from mice treated or not with clonidine (CLD).

a, Schematic representation of the scRNAseq workflow. **b,** UMAP representation of the merged dataset for treated and untreated MC38-OVA tumours. See Supplementary Table 1 for the markers used for cluster identification. **c,** Dotplot representing highly variable genes with

relevance for macrophage activation. See main text for a description of the markers defining clusters 1 and 3. Cluster 2 is characterized by high expression of *Fcer1g, Tyrobp, Cd7, C1qa, C1qb, Cd72, Trem2*, and is similar to the anti-inflammatory macrophages as described before[70]. Cluster 4 is characterized by high expression of *Thbs1, Lgals3, Fn1, Arg1, Ly6c2* and *Tgfbi* and is hence similar to the described population of intermediate monocyte-macrophage[71]. In another paper, these cells were identified as MDSC-like macrophages[72]. Cluster 5 is characterized by a high expression of genes encoding proliferation-related proteins (*Tubb5, Stmn1, Hmgb1, H2afz and Top2a*). **d,** Violin plots (Scanpy) showing the effect of CLD treatment on expression of 10 differentially expressed genes associated with H2 (two-sided Wilcoxon rank sum test with Benjamini-Hochberg correction for multiple testing, p.adj<10-5) in each of the macrophage subpopulations versus the dataset mean. **e,** Enrichment plots (GSEA) in $CD8^+$ T cells indicate an increase in $CD8^+$ T-cell activation, which coincides with an increased $CD8^+$ T cell infiltration shown in Fig. 4b. **f,** Single cell RNAseq analysis of TC-1 lung carcinomas treated or not with CLD. Relative proportions of immune cells in each cluster based on the unsupervised shared nearest-neighbor graph clustering of TC-1 tumours (pools of 10 tumours per group). Class identities were assigned using reference-based cell type annotations using the MC38-OVA tumours (see Fig. 4) as reference. The apparent reduction of macrophages in treated samples is only relative, and results from the increased proportion of $CD4^+$ T cells.

Extended Data Fig 6: Role of macrophages in the anti-tumour effect of α2-AR agonists. **a,** Expression of *Adra2a, Adra2b* and *Adra2c* in macrophages ($CD11b^+$, $F4/80^+$, MHC II^+), PMN-MDSCs ($CD11b^+$, $Gr1^+$ $Ly6G^{high}$ $Ly6C^{low}$) and $CD8^+$ T cells ($CD45^+$ $CD8^+$) sorted from MC38-OVA tumours (a pool of 8 tumours) by BD FACSAria™ III Cell Sorter. Technical duplicates from one representative experiment out of two . **b,** Surface MHC II expression and phagocytic activity of TME macrophages from MC38-OVA tumours in mice treated with vehicle or GBZ. **c,** Surface

MHC II expression of TME macrophages from CT26 tumours in mice treated with vehicle, CLD or GBZ. **d,** Surface MHC II expression (left) and phagocytic activity (right) of TME macrophages from TC-1 tumours in wild-type or *Adra2a-KO* mice treated with vehicle or CLD (n=5 per group). **e,** Efficiency of macrophage depletion by liposomal clodronate. Representative flow cytometry dot plots (left) and statistic bar graph (right) showing the efficacy of macrophage depletion following *in vivo* administration of liposomal clodronate to MC38-OVA tumour-bearing mice, as indicated in Fig. 4f. **f,** Depletion of PMN-MDSCs by liposomal clodronate. The abundance of PMN-MDSCs in tumours was evaluated by flow cytometry following CLD treatment and *in vivo* administration of liposomal clodronate to MC38-OVA tumour-bearing mice. Mean ± s.e.m. n=7, 7, 8, 8 biologically independent samples. **g,** Migration of adoptively transferred $CD45.1^+$ macrophages into lymph nodes and tumours of MC38-OVA tumour-bearing mice (CD45.2). Drugs were administered daily by i.p. injection: GBZ, CLD, 5 mg/kg. Treatments started when tumours reach around 100 mm^3. Mice were sacrificed after 4 days of treatment. **h,** Effect of CLD on the proliferation of murine allogeneic $CD4^+$ and $CD8^+$ T cells co-cultured with WT or *Adra2a*-KO macrophages. T cells were counted by flow cytometry.Technical duplicates from one representative experiment out of three . **i,** Effect of CLD (2.5 μM) on the proliferation of murine OT-II $CD4^+$ and OT-I $CD8^+$ T cells estimated by CFSE dilution after co-culture with WT or *Adra2a*-KO syngeneic macrophages pulsed with ovalbumin protein. An anti-MHC II monoclonal antibody (50 μg/ml) was added as indicated. Technical triplicates from one representative experiment out of three. **j,** Ifn-γ production by OT-I $CD8^+$ T cells co-cultured as in (i**)** and stimulated with E.G7-OVA tumour cells for 16 hours. Intracellular Ifn-γ was measured by flow cytometry. Each dot represents the mean of technical duplicates. n= 4 independent biological replicates. Data (mean ± s.e.m) from one representative experiment out of three (b-f,i) except for g (all mice shown). P values determined by t-test (Unpaired, two-tailed) (b,d,f,i,j). **** $p<0.0001$.

Extended Data Fig 7: Role of $CD4^+$ T cells in the effects of α2-AR agonists.

a, Representative flow cytometry dot plots showing the efficacy of $CD4^+$ T-cell depletion following *in vivo* administration of the anti-CD4 mAb in tumour (left) and spleen (right). **b**, Progression of TC-1 tumours in mice treated with CLD, anti-CD4, or both. **c,** Infiltration of $CD4^+$ and $CD8^+$ T cells in the tumour, lymph node and spleen of TC-1 tumour-bearing mice treated with CLD, anti-CD4, or both. The apparently increased $CD8^+$ T cell proportion in CD4-depleted samples is only relative, and so appears because of the disappearance of $CD4^+$ T cells in those samples. **d and e**, Progression of TC-1 (d) or MC38-OVA (e) tumours in mice treated with CLD, anti-MHC II, or both. CLD was given daily (5 mg/kg i.p.) starting at day 0 when tumours reached the indicated size. Anti-CD4 antibody (500 μg) was given 1 day before starting CLD treatment, then 250 μg twice per week. Anti-MHC II (500 μg) antibody (i.p.) was given 1 day before the first injection of CLD, then twice a week. Data (mean ± s.e.m) from one representative out of three independent experiments (c) except for b, d and e (all mice shown). P values determined by: ordinary two-way ANOVA (b, d, e), t-test (Unpaired, two-tailed) (c). **** $p<0.0001$.

Extended Data Fig 8: Effects of α2-AR agonists on the cAMP-PKA signaling pathway.

a, MC38-tumour bearing mice (10 mice per group) were treated with CLD or vehicle for 7 days. Tumours and lymph nodes were collected and pooled for isolation of $CD11b^+$ cells. Left panels: Cell lysates were analyzed for phospho-CREB and total CREB by western blotting. Beta-actin was used as loading control. The phospho-CREB to total CREB ratio is indicated below the blots. Right panels: MHC II expression of $CD11b^+$ cells in the lymph nodes and tumours from the same mice used in the left panels. **b,** Quantification of cAMP levels in *in vitro* differentiated M1 macrophages treated with different concentrations of CLD for 15 minutes. Mean ± s.e.m of

one experiment (technical triplicates). **c,** M1 macrophages differentiated *in vitro* from WT or *Adra2a*-KO bone marrow cells were treated with CLD (2.5 μM) for 16 hours. Cell lysates were then analyzed for phospho-CREB and total CREB by western blotting (left panels). Macrophages treated with PKA inhibitor (H-89 dihydrochloride hydrate, 1 μM) were used as controls. Beta-actin was used as loading control. The phospho-CREB to total CREB ratio is indicated below the blots. MHC II expression by the same cells is shown on the right panel. For gel source data, see Supplementary Figure 1b and c. Data (mean ± s.e.m) from one representative out of two independent experiments (a,c). P values determined by *t*-test (Unpaired, two-tailed). **** $p<0.0001$.

Extended Data Fig 9: Association of α2-AR tumour signaling with survival of cancer patients.

a, Kaplan–Meier curves for Overall Survival (OS) and Progression-free Survival (PFS) related to *ADRA2* metagene (sum of *ADRA2A, ADRA2B, ADRA2C*) expression in human lung adenocarcinoma (LUAD) analyzed using clinical data from TCGA (n=515). **b,** Heatmap showing correlation of the expression of immune modulators genes with *ADRA2* metagene expression across the TCGA cancer types (30 cancer types; ACC: n=77, BLCA: n=413, BRCA: n=1130, CESC: n=304, COAD: n=331, ESCA: n=181, GBM: n=158, HNSC: n=518, KICH: n=66, KIRC: n=542, KIRP: n=288, LGG: n=508, LIHC: n=369, LUAD: n=537, LUSC: n=503, MESO: n=87, OV: n=423, PAAD: n=178, PCPG: n=176, PRAD: n=503, READ: n=91, SARC: n=258, SKCM: n=102, STAD: n=414, TGCT: n=132, THCA: n=504, THYM: n=119, UCEC: n=189, UCS: n=57, UVM: n=79). **c,** Heatmaps showing the expression fold changes of genes downregulated (Post_Down) or upregulated (Post_Up) by CLD and GBZ in MC38-OVA tumours from WT or *Adra2a*-KO mice, as compared to untreated tumours (6 conditions, n=3 per group)**. d,** Cox Proportional Hazards (CoxPH) regression analysis across clinical trials in

TIDE[37,38] (BLCA: n=348, SKCM: n=41), using as input the human ortholog genes of the up- and downregulated gene signatures post treatment with CLD or GBZ (Post_Up and Post_Down). Negative Z-scores indicate better survival in the high expression group per signature. **e,** Boxplots highlighting statistically significant differences between high and low expression of the Post_Up and Post_Down gene signatures across a set of immune parameters calculated for TCGA (n=9320, 30 cancer types). Groups were selected based on median expression of Post_Up or Post_Down signatures. Boxes represent the median, 1st and 3rd quartiles; outliers were determined based on the interquartile range and ignored for visualization. P values are determined by Log-rank-test (a), CoxPh regression-test (d), Two-sidedWelch *t*-tests (e). $p<0.05$ is considered significant.

Extended Data Fig 10: Anti-tumour effect of clonidine administered via the oral route (a,b), and schematic model of the anti-tumour activity of α2-AR agonists (c) .

a, Progression of MC38-OVA colon carcinomas in mice treated with drinking water supplemented with clonidine (CLD) (10 μg/ml). **b**, Phagocytic activity of TME macrophages from mice treated in (a) (n=8 per group). Data (mean ± s.e.m) from one representative out of three independent experiments. P values determined by ordinary two-way ANOVA (left) and *t*-test (Unpaired, two-tailed, right). **** $p<0.0001$. **c,** Model of the identified mechanisms underlying the anti-tumour activity of α2-AR agonists in the context of immunotherapy. Tumour-associated macrophages and myeloid-derived suppressor cells (MDSCs) contribute to immunosuppression in the tumour microenvironment, partly in response to factors such as adenosine and prostaglandins, which trigger the cAMP/pCREB signaling pathway. Agonists of the α2-adrenergic receptor (blue) inhibit adenylate cyclase (AC), thereby blocking the immunosuppressive cAMP/pCREB signaling. Macrophages now better stimulate anti-tumour CD4 and CD8 T cells, while MDSCs die by apoptosis. (Created with BioRender.com)

References:

70 Poon, C. C. *et al.* Differential microglia and macrophage profiles in human IDH-mutant and -wild type glioblastoma. *Oncotarget* **10**, 3129-3143, doi:10.18632/oncotarget.26863 (2019).

71 Ochocka, N. *et al.* Single-cell RNA sequencing reveals functional heterogeneity of glioma-associated brain macrophages. *Nature communications* **12**, 1151, doi:10.1038/s41467-021-21407-w (2021).

72 Zhang, Q. *et al.* Landscape and Dynamics of Single Immune Cells in Hepatocellular Carcinoma. *Cell* **179**, 829-845 e820, doi:10.1016/j.cell.2019.10.003 (2019).

Figure 1

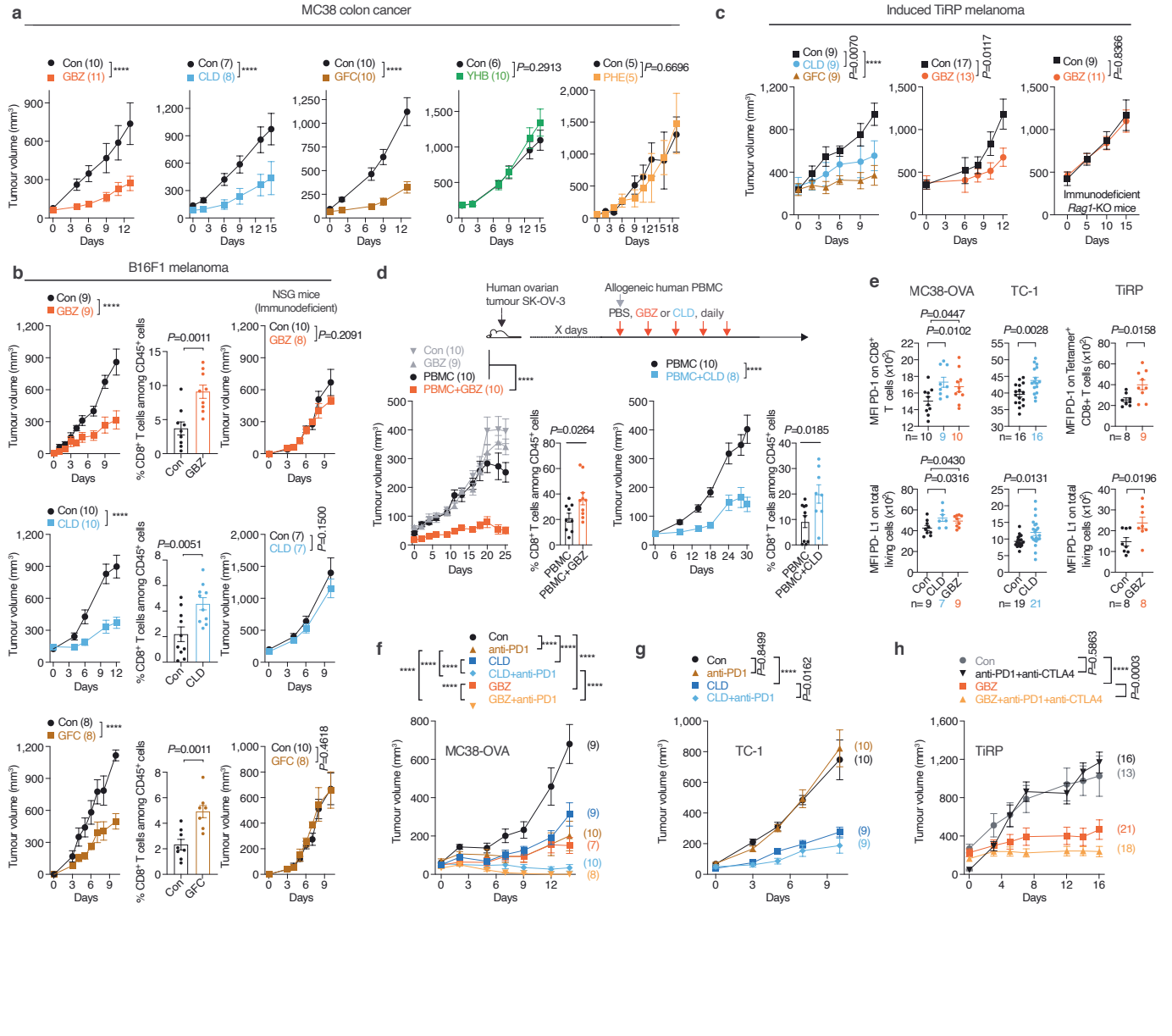
a
MC38 colon cancer
Con (10)
GBZ (11)
****
Con (7)
CLD (8)
****
Con (10)
GFC(10)
****
Con (6)
YHB (10)
P=0.2913
Con (5)
PHE(5)
P=0.6696
Tumour volume (mm³)
Days
c
Induced TiRP melanoma
Con (9)
CLD (9)
GFC (9)
P=0.0070
****
Con (17)
GBZ (13)
P=0.0117
Con (9)
GBZ (11)
P=0.8366
Immunodeficient
Rag1-KO mice
b
B16F1 melanoma
Con (9)
GBZ (9)
****
P=0.0011
% CD8⁺ T cells among CD45⁺ cells
Con
GBZ
NSG mice
(Immunodeficient)
Con (10)
GBZ (8)
P=0.2091
Con (10)
CLD (10)
****
P=0.0051
Con
CLD
Con (7)
CLD (7)
P=0.1500
Con (8)
GFC (8)
****
P=0.0011
Con
GFC
Con (10)
GFC (8)
P=0.4618
d
Human ovarian
tumour SK-OV-3
Allogeneic human PBMC
PBS, GBZ or CLD, daily
X days
Con (10)
GBZ (9)
PBMC (10)
PBMC+GBZ (10)
****
P=0.0264
PBMC
PBMC+GBZ
PBMC (10)
PBMC+CLD (8)
****
P=0.0185
PBMC
PBMC+CLD
e
MC38-OVA
TC-1
TiRP
P=0.0447
P=0.0102
P=0.0028
P=0.0158
MFI PD-1 on CD8⁺ T cells (x10⁵)
n= 10 9 10
n= 16 16
n= 8 9
MFI PD-1 on Tetramer⁺ CD8+ T cells (x10⁵)
P=0.0430
P=0.0316
P=0.0131
P=0.0196
MFI PD- L1 on total living cells (x10⁵)
Con
CLD
GBZ
n= 9 7 9
n= 19 21
n= 8 8
f
Con
anti-PD1
CLD
CLD+anti-PD1
GBZ
GBZ+anti-PD1
****
MC38-OVA
(9)
(9)
(10)
(7)
(10)
(8)
g
Con
anti-PD1
CLD
CLD+anti-PD1
P=0.8499
****
P=0.0162
TC-1
(10)
(10)
(9)
(9)
h
Con
anti-PD1+anti-CTLA4
GBZ
GBZ+anti-PD1+anti-CTLA4
P=0.5863
****
P=0.0003
TiRP
(16)
(13)
(21)
(18)
Days

Figure 2

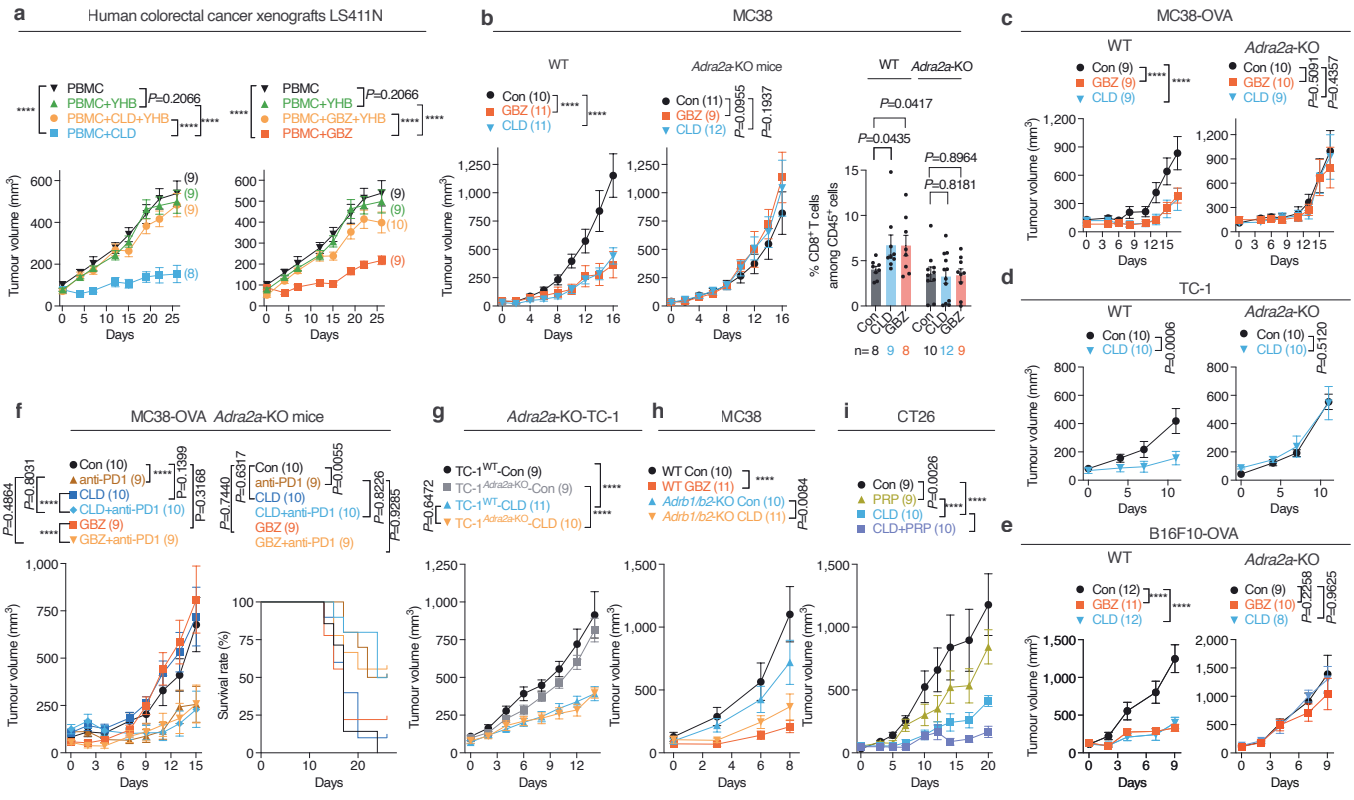
a
Human colorectal cancer xenografts LS411N
PBMC
PBMC+YHB
PBMC+CLD+YHB
PBMC+CLD
P=0.2066
PBMC+GBZ+YHB
PBMC+GBZ
Tumour volume (mm3)
Days
b
MC38
WT
Adra2a-KO mice
Con (10)
GBZ (11)
CLD (11)
Con (11)
GBZ (9)
CLD (12)
P=0.0955
P=0.1937
% CD8+ T cells among CD45+ cells
P=0.0417
P=0.0435
P=0.8964
P=0.8181
n= 8 9 8 10 12 9
c
MC38-OVA
Con (9)
GBZ (9)
CLD (9)
Con (10)
GBZ (10)
CLD (9)
P=0.3091
P=0.4357
d
TC-1
Con (10)
CLD (10)
P=0.0006
P=0.5120
e
B16F10-OVA
Con (12)
GBZ (11)
CLD (12)
Con (9)
GBZ (10)
CLD (8)
P=0.2258
P=0.9625
f
MC38-OVA Adra2a-KO mice
Con (10)
anti-PD1 (9)
CLD (10)
CLD+anti-PD1 (10)
GBZ (9)
GBZ+anti-PD1 (9)
P=0.4864
P=0.8031
P=0.1399
P=0.3168
P=0.7440
P=0.6317
P=0.0055
P=0.8226
P=0.9285
Survival rate (%)
g
Adra2a-KO-TC-1
TC-1WT-Con (9)
TC-1Adra2a-KO-Con (9)
TC-1WT-CLD (11)
TC-1Adra2a-KO-CLD (10)
P=0.6472
h
MC38
WT Con (10)
WT GBZ (11)
Adrb1/b2-KO Con (10)
Adrb1/b2-KO CLD (11)
P=0.0084
i
CT26
Con (9)
PRP (9)
CLD (10)
CLD+PRP (10)
P=0.0026

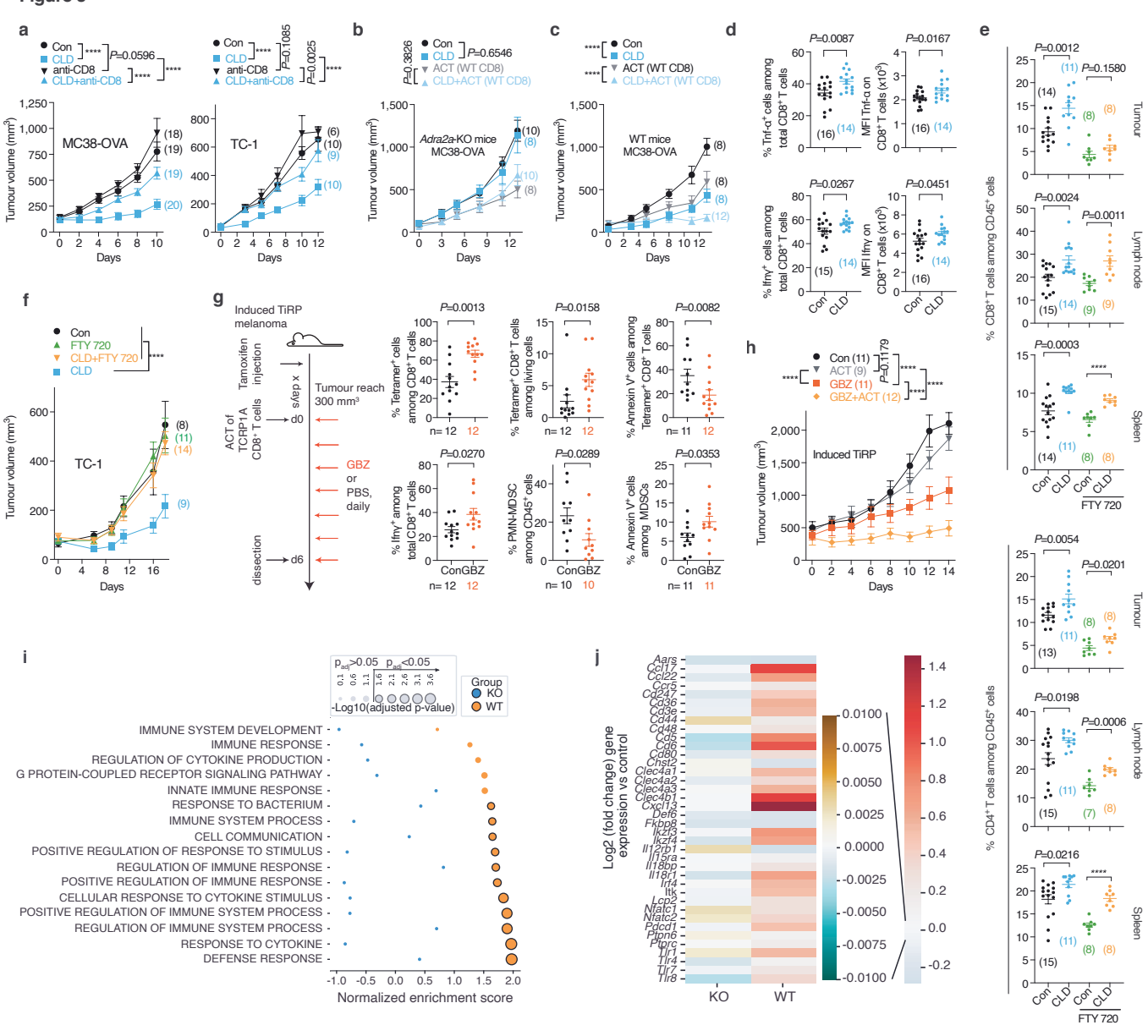
Figure 3
a
Con
CLD
anti-CD8
CLD+anti-CD8
P=0.0596
P=0.1085
P=0.0025
MC38-OVA
TC-1
Tumour volume (mm3)
Days
b
P=0.3826
P=0.6546
ACT (WT CD8)
CLD+ACT (WT CD8)
Adra2a-KO mice
MC38-OVA
c
WT mice
MC38-OVA
d
P=0.0087
P=0.0167
% Tnf-α+ cells among total CD8+ T cells
MFI Tnf-α on CD8+ T cells (x10³)
P=0.0267
P=0.0451
% Ifnγ+ cells among total CD8+ T cells
MFI Ifnγ on CD8+ T cells (x10³)
Con
CLD
e
P=0.0012
P=0.1580
P=0.0024
P=0.0011
P=0.0003
Tumour
Lymph node
Spleen
% CD8+ T cells among CD45+ cells
FTY 720
P=0.0054
P=0.0201
P=0.0198
P=0.0006
P=0.0216
% CD4+ T cells among CD45+ cells
f
Con
FTY 720
CLD+FTY 720
CLD
TC-1
g
Induced TiRP melanoma
Tamoxifen injection
sAep x
ACT of TCRP1A CD8+ T cells
d0
d6
dissection
Tumour reach 300 mm3
GBZ or PBS, daily
P=0.0013
P=0.0158
P=0.0082
% Tetramer+ cells among CD8+ T cells
% Tetramer+ CD8+ T cells among living cells
% Annexin V+ cells among Tetramer+ CD8+ T cells
P=0.0270
P=0.0289
P=0.0353
% Ifnγ+ among total CD8+ T cells
% PMN-MDSC among CD45+ cells
% Annexin V+ cells among MDSCs
Con
GBZ
h
Con (11)
ACT (9)
GBZ (11)
GBZ+ACT (12)
P=0.1179
Induced TiRP
i
padj>0.05
padj<0.05
-Log10(adjusted p-value)
Group
KO
WT
IMMUNE SYSTEM DEVELOPMENT
IMMUNE RESPONSE
REGULATION OF CYTOKINE PRODUCTION
G PROTEIN-COUPLED RECEPTOR SIGNALING PATHWAY
INNATE IMMUNE RESPONSE
RESPONSE TO BACTERIUM
IMMUNE SYSTEM PROCESS
CELL COMMUNICATION
POSITIVE REGULATION OF RESPONSE TO STIMULUS
REGULATION OF IMMUNE RESPONSE
POSITIVE REGULATION OF IMMUNE RESPONSE
CELLULAR RESPONSE TO CYTOKINE STIMULUS
POSITIVE REGULATION OF IMMUNE SYSTEM PROCESS
REGULATION OF IMMUNE SYSTEM PROCESS
RESPONSE TO CYTOKINE
DEFENSE RESPONSE
Normalized enrichment score
j
Log2 (fold change) gene expression vs control
Aars
Ccl17
Ccl22
Ccr5
Cd247
Cd36
Cd3e
Cd44
Cd48
Cd6
Cd80
Chst2
Clec4a1
Clec4a2
Clec4a3
Clec4b1
Cxcl13
Def6
Fkbp8
Ikzf3
Ikzf4
Il12rb1
Il15ra
Il18bp
Il18r1
Irf4
Itk
Lcp2
Ntatc1
Ntatc2
Ptdc1
Ptpn6
Ptprc
Tlr1
Tlr4
Tlr7
Tlr8
KO
WT

Figure 4

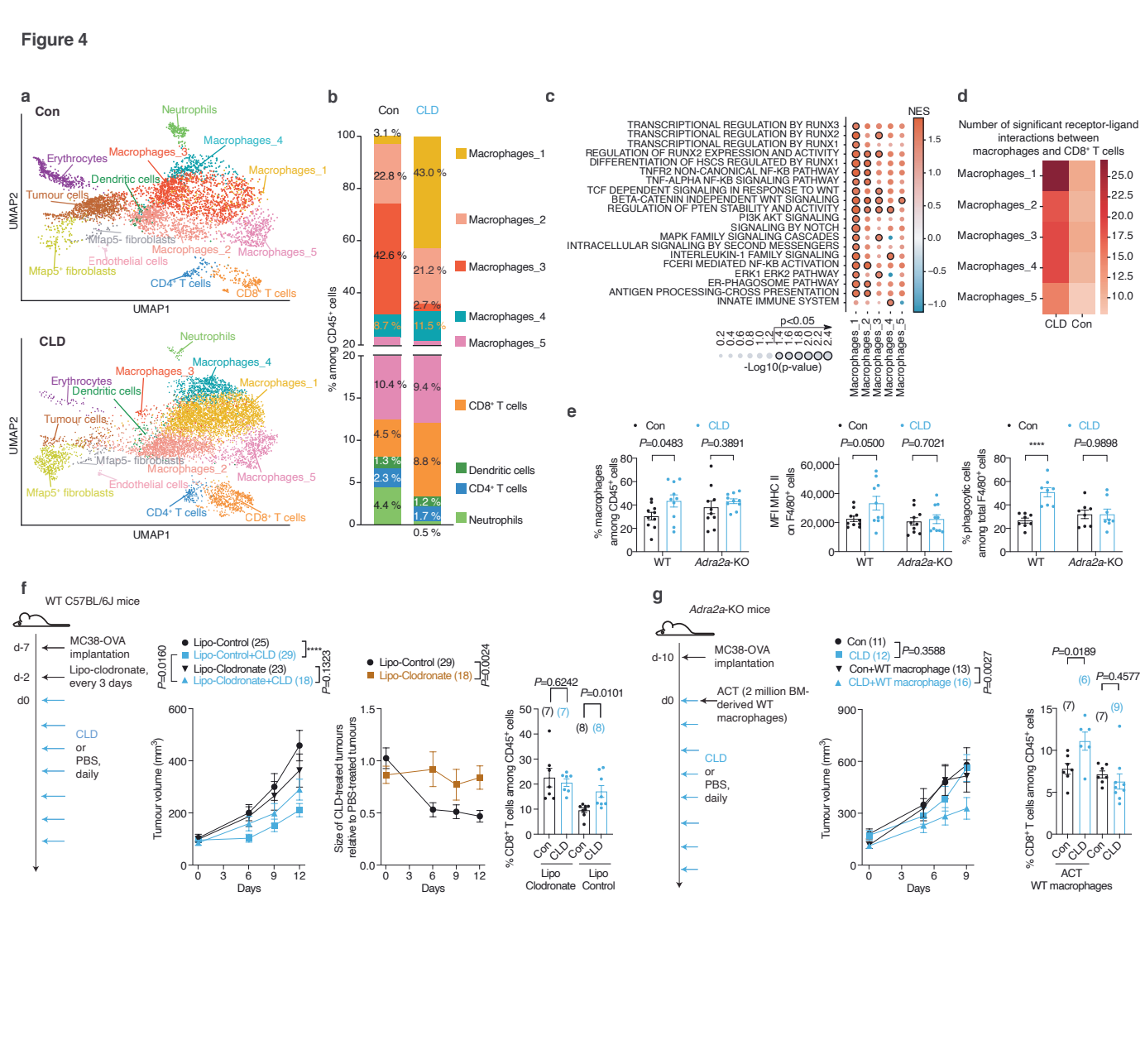
a
Con
Neutrophils
Macrophages_4
Macrophages_3
Erythrocytes
Macrophages_1
Dendritic cells
Tumour cells
Mfap5- fibroblasts
Macrophages_2
Macrophages_5
Endothelial cells
Mfap5+ fibroblasts
CD4+ T cells
CD8+ T cells
UMAP2
UMAP1
CLD
Neutrophils
Macrophages_4
Macrophages_3
Erythrocytes
Macrophages_1
Dendritic cells
Tumour cells
Mfap5- fibroblasts
Macrophages_2
Macrophages_5
Endothelial cells
Mfap5+ fibroblasts
CD4+ T cells
CD8+ T cells
UMAP2
UMAP1
b
Con
CLD
% among CD45+ cells
3.1 %
22.8 %
42.6 %
3.7 %
43.0 %
21.2 %
2.7 %
11.5 %
10.4 %
4.5 %
1.3 %
2.3 %
4.4 %
9.4 %
8.8 %
1.2 %
1.7 %
0.5 %
Macrophages_1
Macrophages_2
Macrophages_3
Macrophages_4
Macrophages_5
CD8+ T cells
Dendritic cells
CD4+ T cells
Neutrophils
c
TRANSCRIPTIONAL REGULATION BY RUNX3
TRANSCRIPTIONAL REGULATION BY RUNX2
TRANSCRIPTIONAL REGULATION BY RUNX1
REGULATION OF RUNX2 EXPRESSION AND ACTIVITY
DIFFERENTIATION OF HSCS REGULATED BY RUNX1
TNFR2 NON-CANONICAL NF-KB PATHWAY
TNF-ALPHA NF-KB SIGNALING PATHWAY
TCF DEPENDENT SIGNALING IN RESPONSE TO WNT
BETA-CATENIN INDEPENDENT WNT SIGNALING
REGULATION OF PTEN STABILITY AND ACTIVITY
PI3K AKT SIGNALING
SIGNALING BY NOTCH
MAPK FAMILY SIGNALING CASCADES
INTRACELLULAR SIGNALING BY SECOND MESSENGERS
INTERLEUKIN-1 FAMILY SIGNALING
FCERI MEDIATED NF-KB ACTIVATION
ERK1 ERK2 PATHWAY
ER-PHAGOSOME PATHWAY
ANTIGEN PROCESSING-CROSS PRESENTATION
INNATE IMMUNE SYSTEM
NES
p<0.05
-Log10(p-value)
Macrophages_1
Macrophages_2
Macrophages_3
Macrophages_4
Macrophages_5
d
Number of significant receptor-ligand interactions between macrophages and CD8+ T cells
Macrophages_1
Macrophages_2
Macrophages_3
Macrophages_4
Macrophages_5
CLD
Con
e
Con
CLD
P=0.0483
P=0.3891
% macrophages among CD45+ cells
P=0.0500
P=0.7021
MFI MHC II on F4/80+ cells
****
P=0.9898
% phagocytic cells among total F4/80+ cells
WT
Adra2a-KO
f
WT C57BL/6J mice
d-7
MC38-OVA implantation
d-2
Lipo-clodronate, every 3 days
d0
CLD or PBS, daily
Lipo-Control (25)
Lipo-Control+CLD (29)
Lipo-Clodronate (23)
Lipo-Clodronate+CLD (18)
P=0.0160
****
P=0.1323
Tumour volume (mm3)
Days
Lipo-Control (29)
Lipo-Clodronate (18)
P=0.0024
Size of CLD-treated tumours relative to PBS-treated tumours
Days
P=0.6242
P=0.0101
(7)
(7)
(8)
(8)
% CD8+ T cells among CD45+ cells
Con
CLD
Con
CLD
Lipo Clodronate
Lipo Control
g
Adra2a-KO mice
d-10
MC38-OVA implantation
d0
ACT (2 million BM-derived WT macrophages)
CLD or PBS, daily
Con (11)
CLD (12)
Con+WT macrophage (13)
CLD+WT macrophage (16)
P=0.3588
P=0.0027
Tumour volume (mm3)
Days
P=0.0189
P=0.4577
(7)
(6)
(7)
(9)
% CD8+ T cells among CD45+ cells
Con
CLD
Con
CLD
ACT
WT macrophages

Extended Data Figure 1

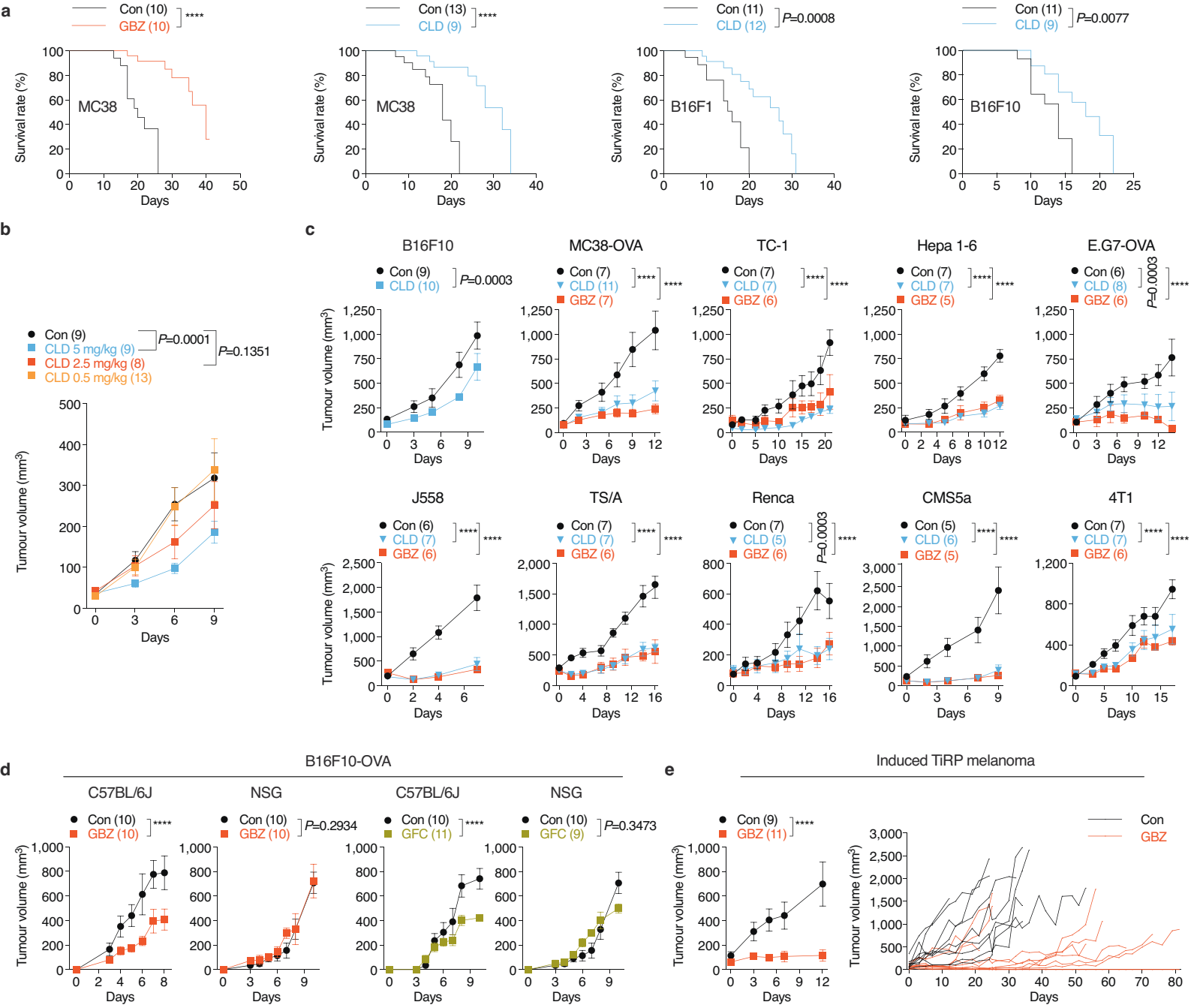

Extended Data Figure 2

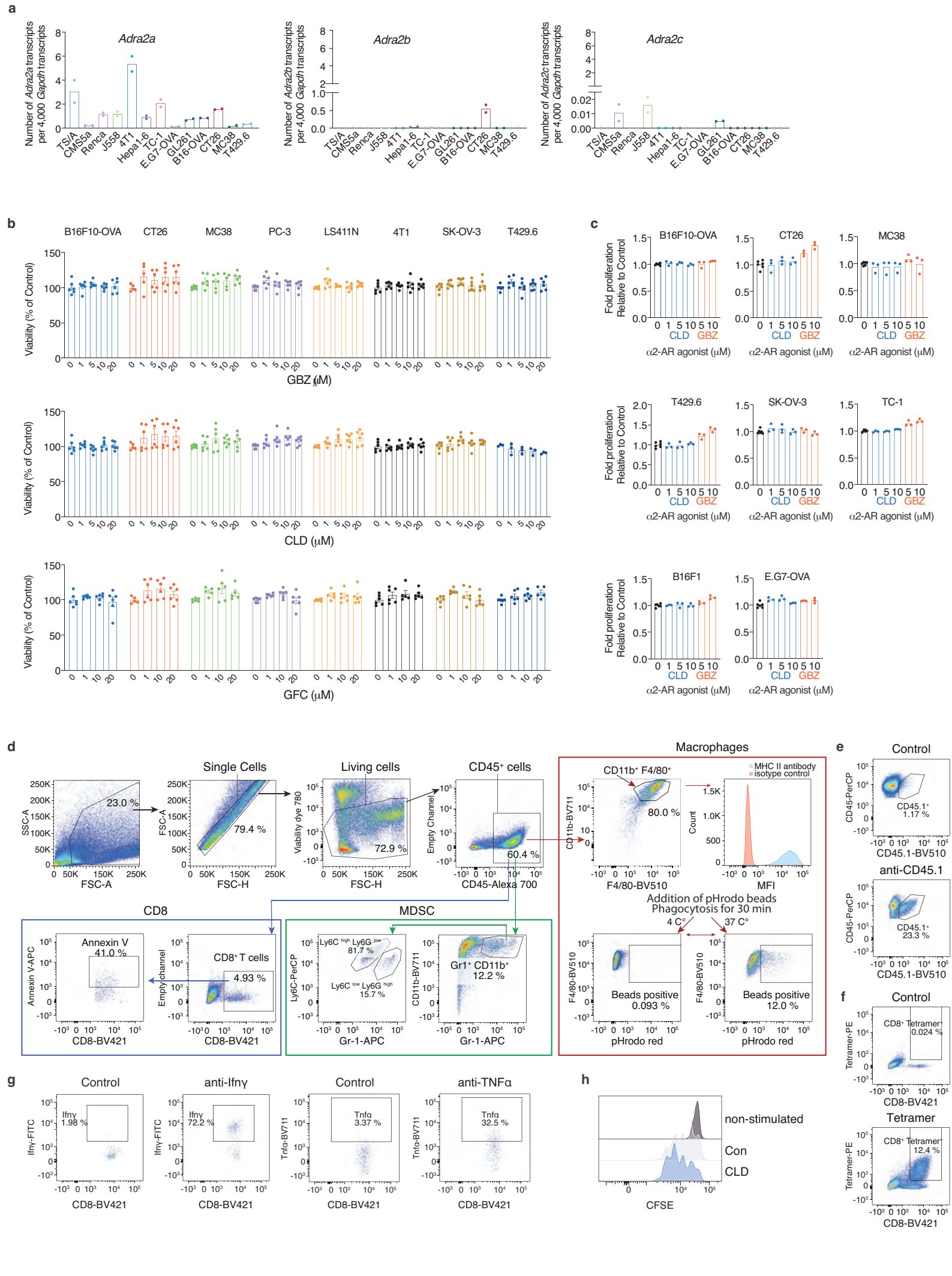

Extended Data Figure 3

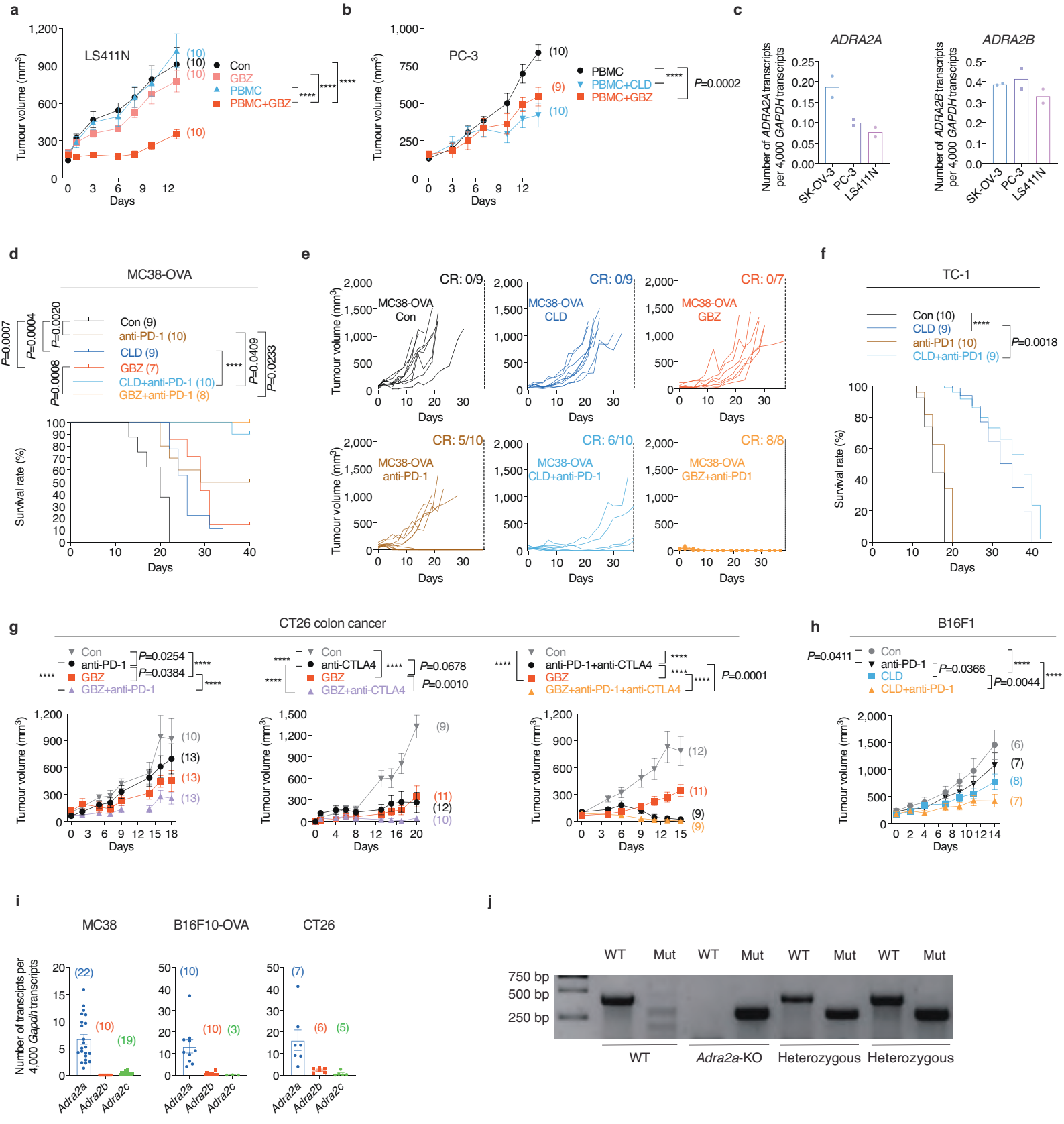

Extended Data Figure 4

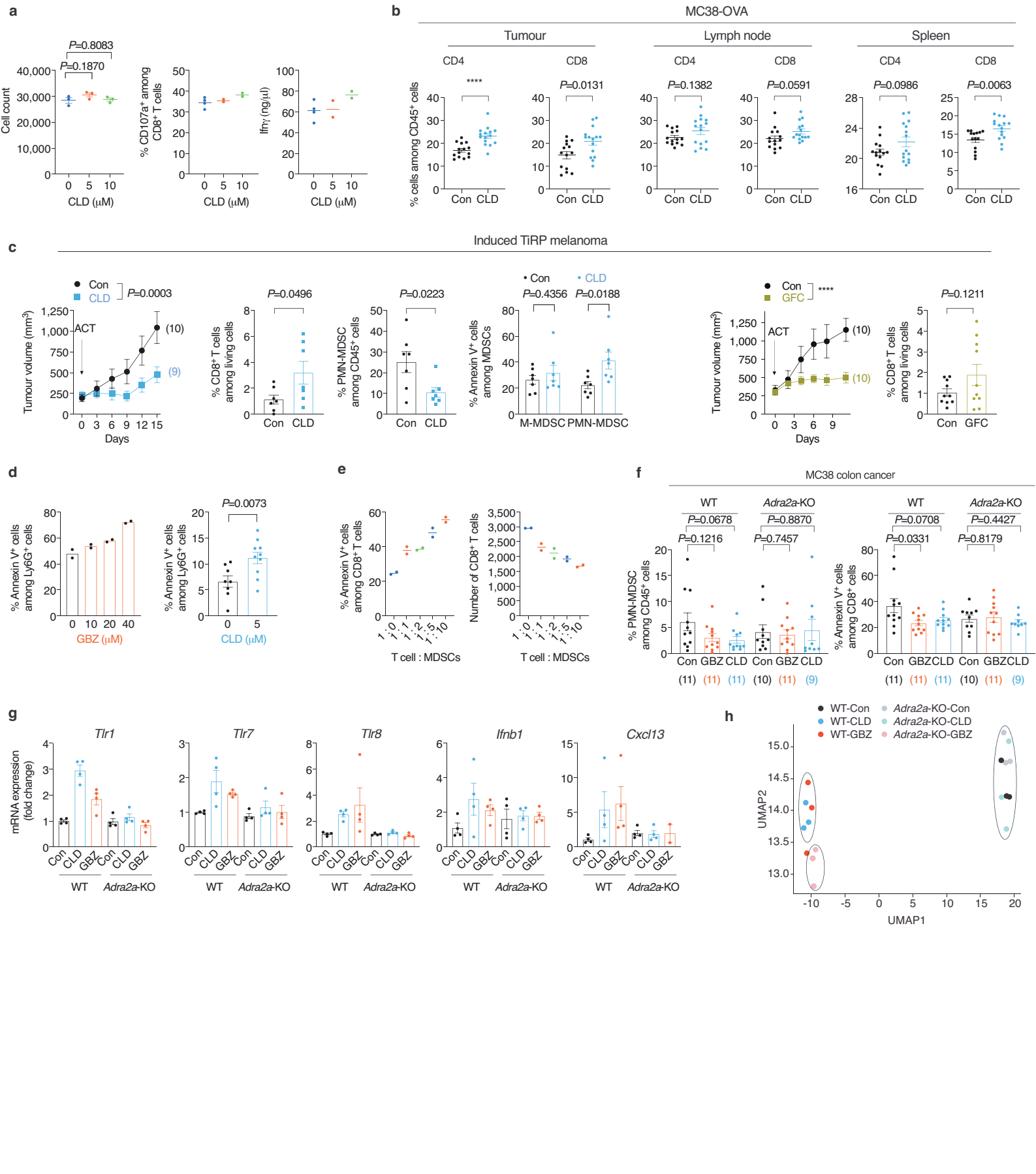

Extended Data Figure 5

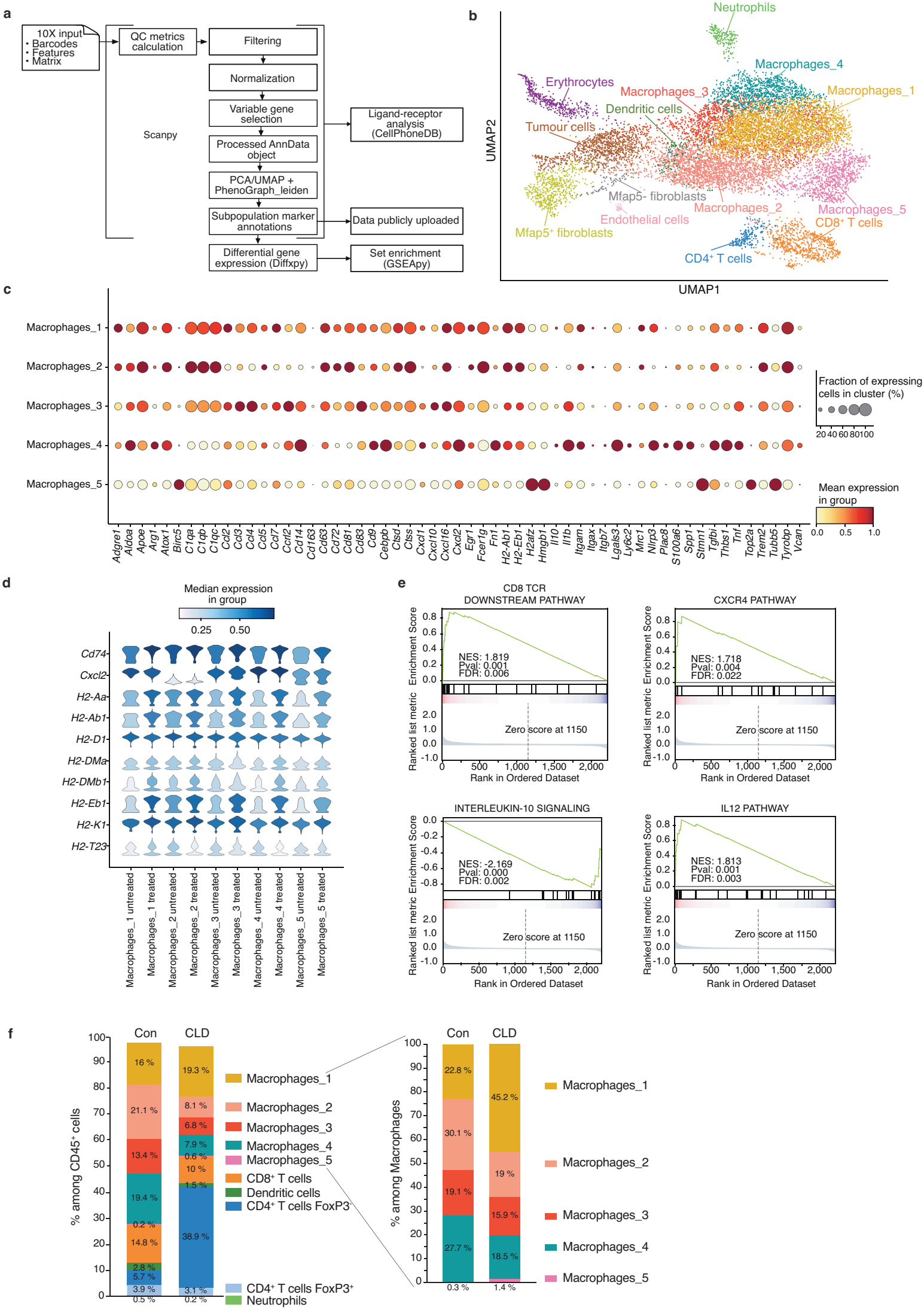

Extended Data Figure 6

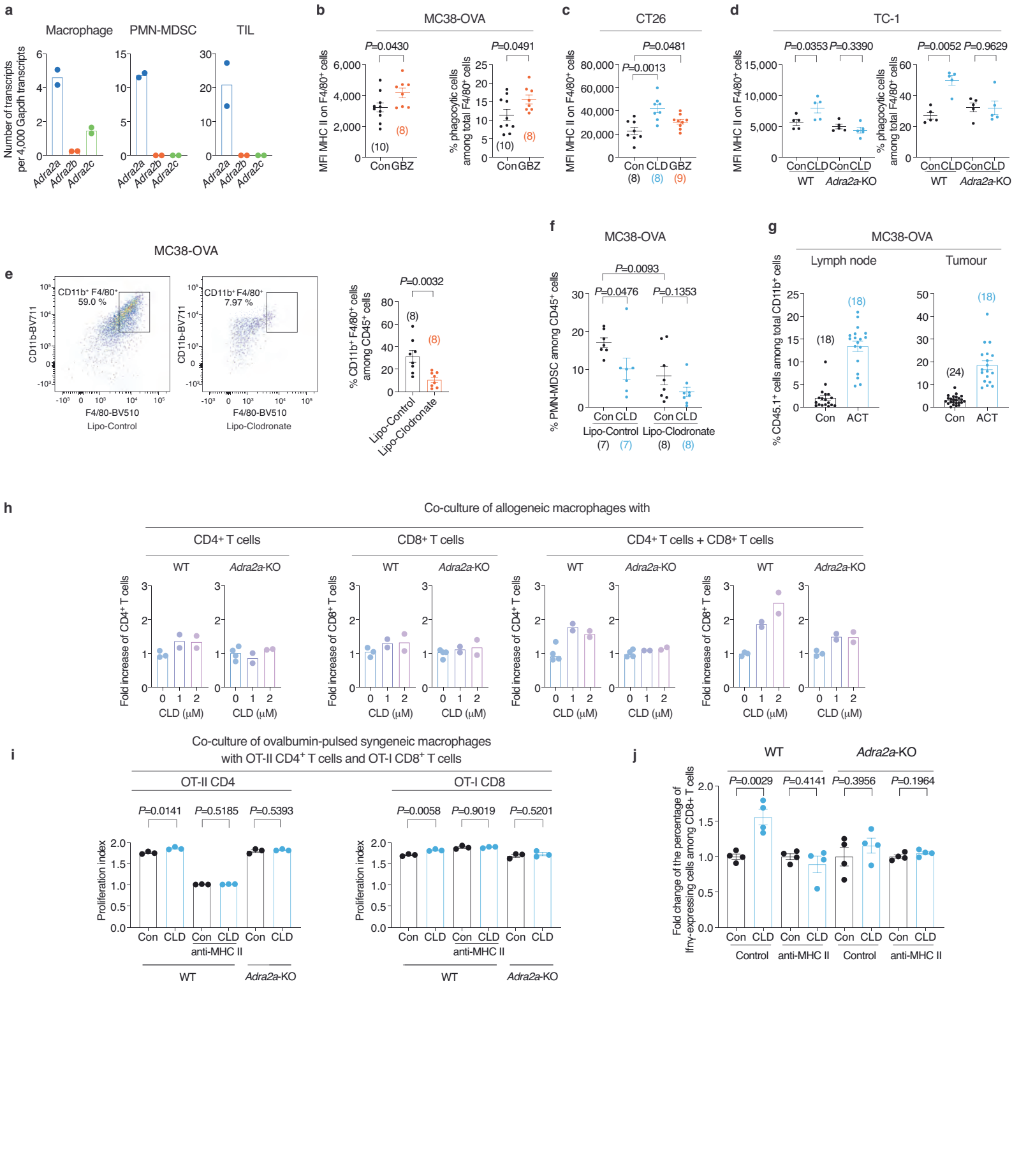

Extended Data Figure 7

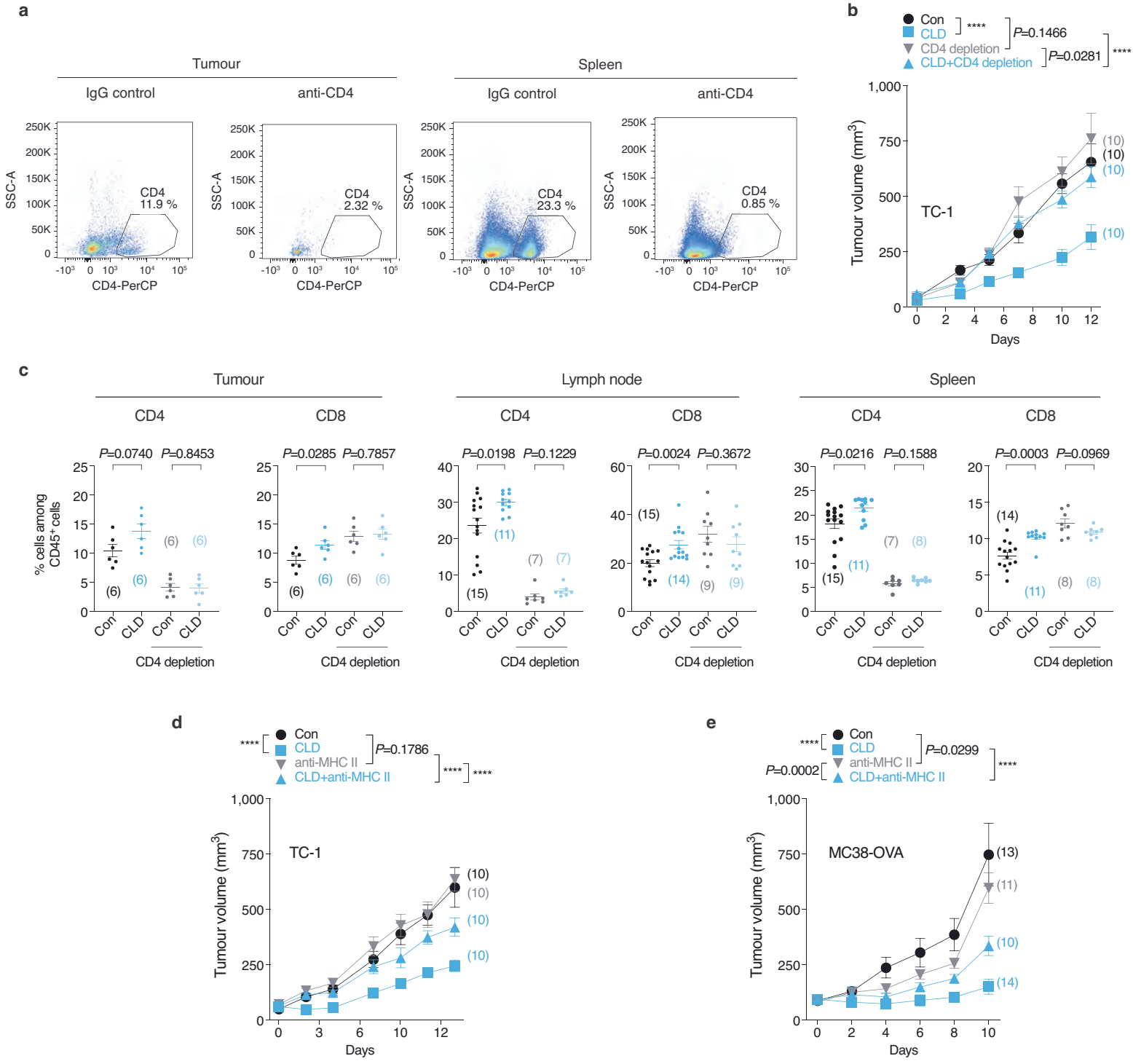

Extended Data Figure 8

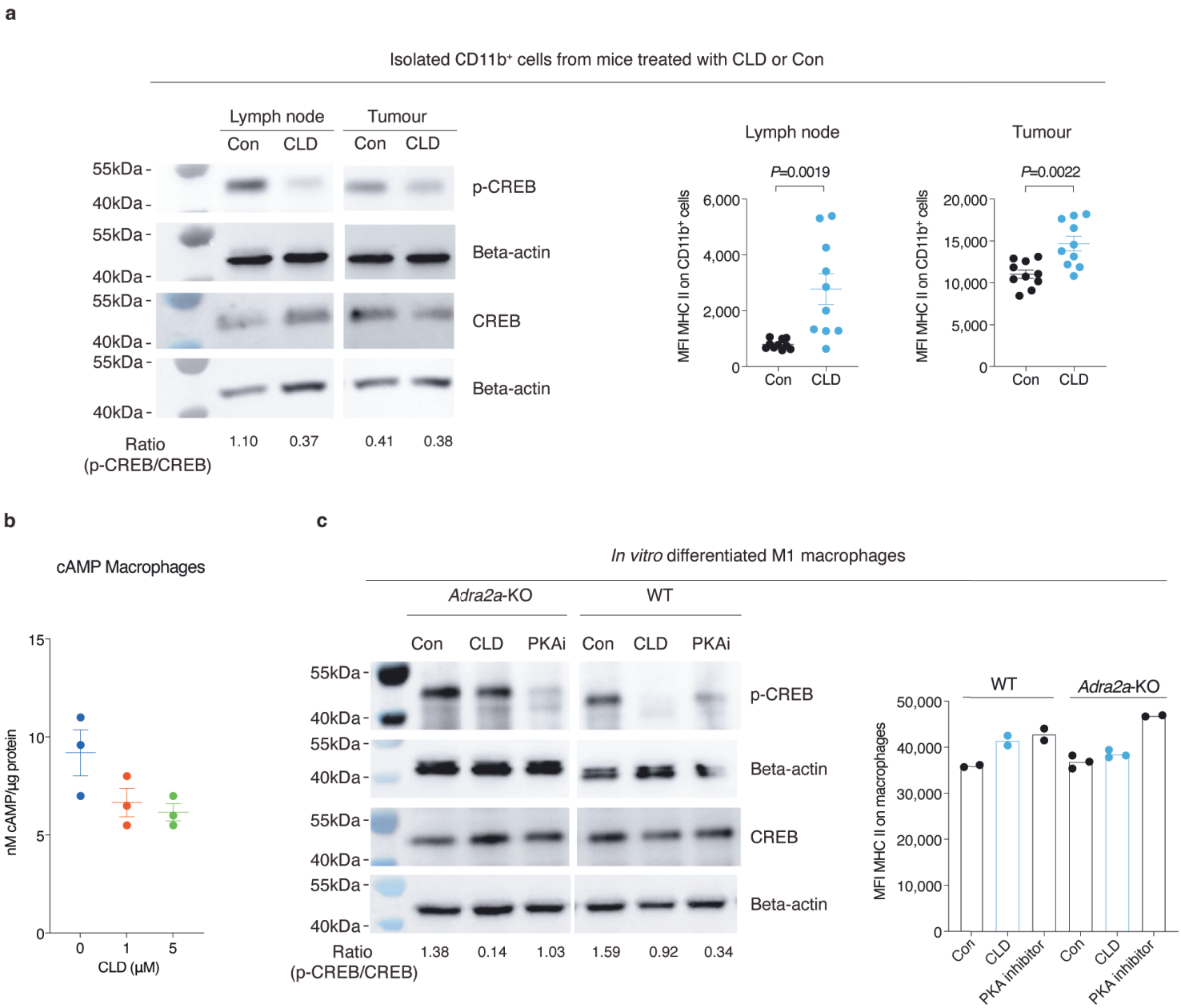

Extended Data Figure 9

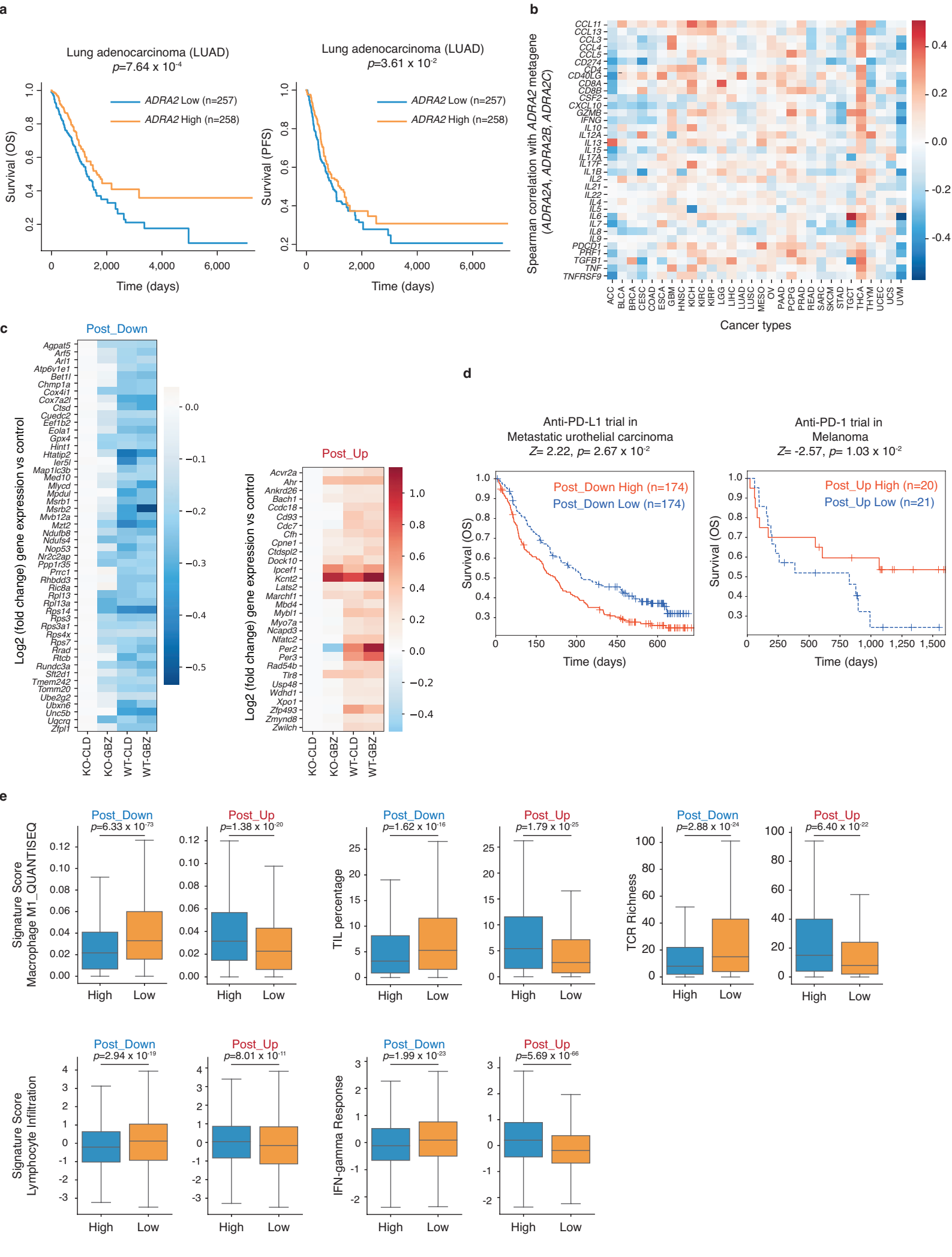

Extended Data Figure 10